https://doi.org/10.5194/hess-2020-493
Preprint. Discussion started: 13 October 2020

Hydrology and Earth System Sciences
Discussions

The role of dew and radiation fog inputs in the local water cycling of a temperate grassland in Central Europe

Yafei Li[1], Franziska Aemisegger[2], Andreas Riedl[1], Nina Buchmann[1], Werner Eugster[1]

[1]Institute of Agricultural Sciences, ETH Zurich, Zurich Switzerland
[2]Institute for Atmospheric and Climate Science, ETH Zurich, Zurich, Switzerland

Correspondence to: Yafei Li (yafei.li@usys.ethz.ch); Werner Eugster (werner.eugster@usys.ethz.ch)

Abstract. In a warmer climate, non-rainfall water (hereafter NRW) formed from dew and fog potentially plays an increasingly important role in temperate grassland ecosystems under the scarcity of precipitation over prolonged periods. Dew and radiation fog occur in combination during clear and calm nights, and both use ambient water vapor as a source. Research on the combined mechanisms involved in NRW inputs to ecosystems are rare, and the condensation of soil-diffusing vapor, as one of the NRW input pathways for dew formation, has hardly been studied at all. The aim of this paper is thus to investigate the different NRW input pathways into a temperate Swiss grassland at Chamau during prolonged dry periods in summer 2018. We measured the isotopic compositions ($\delta^{18}O$, $\delta^{2}H$, and $d = \delta^{2}H - 8 \cdot \delta^{18}O$) of both ambient water vapor and the NRW droplets on leaf surfaces combined with eddy covariance and meteorological measurements during one dew-only and two combined dew and radiation fog events. We employed a simple two end-member mixing model using $\delta^{18}O$ and $\delta^{2}H$ to split the dew input pathways from different sources. Our results showed a decrease of 0.8–5.5 mmol mol^{-1} in volumetric water vapor mixing ratio and a decrease of 4.8–16.7‰ in ambient water vapor $\delta^{2}H$ due to dew formation and radiation fog droplet deposition. A nighttime maximum in ambient water vapor $\delta^{18}O$ (–15.5‰ to –14.3‰) and a 3.4–3.7‰ decrease in ambient water vapor d were observed for dew formation in unsaturated conditions. In conditions of slight super-saturation, a stronger decrease of ambient water vapor $\delta^{18}O$ (0.3–1.5‰) and a minimum of ambient water vapor d (–6.0‰ to –4.7‰) were observed. The combined foliage NRW and ambient water vapor $\delta^{18}O$ and $\delta^{2}H$ suggested two different input pathways: (1) condensation of ambient water vapor and (2) of soil-diffusing vapor. The latter contributed 9–42 % to the total foliage NRW. The dew and radiation fog potentially produced 0.06–0.39 mm night^{-1} NRW gain on foliage, which was comparable with 2.8 mm day^{-1} daytime evapotranspiration. The ambient water vapor d was correlated and anti-correlated with ambient temperature and ambient relative humidity respectively, suggesting an only minor influence of large-scale air advection and highlighted the dominant role of local moisture as a source for ambient water vapor. Our results thus highlight the importance of NRW inputs to temperate grasslands during prolonged dry periods and reveal the complexity of the local water cycle in such conditions including different pathways of water deposition.

1 Introduction

During extended periods without rainfall, non-rainfall water (hereafter NRW) inputs, namely dew and fog, are an essential water source for plants in arid and semi-arid regions (Agam and Berliner, 2006; del Prado and Sancho, 2007; He and Richards, 2015; Jacobs et al., 2002; Kidron et al., 2002; Malek et al., 1999; McHugh et al., 2015; Tomaszkiewicz et al., 2017; Ucles et al., 2013), Mediterranean coastal regions (Beysens et al., 2007), temperate ecosystems (Jacobs et al., 2006), and tropical climates (Clus et al., 2008). In clear calm nights when dew and radiation fog occur, the atmospheric boundary layer becomes stably stratified, leading to a shallow stable nocturnal boundary layer (hereafter NBL) with a depth on the order of no more than 50–100 m (Garratt, 1992). Dew and radiation fog occur at the bottom of the NBL (Garratt, 1992; Monteith and Unsworth, 2013; Oke, 2002; Stull, 1988). Both dew and radiation fog are formed due to the cooling of the Earth's surface after sunset by

https://doi.org/10.5194/hess-2020-493
Preprint. Discussion started: 13 October 2020


Hydrology and Earth System Sciences
Discussions

long-wave radiation losses in clear nights (Oke, 2002). This radiative cooling is a process due to which a body loses heat by long-wave thermal radiation, whereby its surface cools down below the dew point of the adjacent air. Under such conditions, dew can form on plant surfaces while fog forms on activated aerosol particles in the near-surface atmosphere.

NRW inputs contribute to the water budget across many ecosystems including croplands (Atzema et al., 1990; Meng and Wen, 2016; Tomaszkiewicz et al., 2017; Wen et al., 2012), grasslands (He and Richards, 2015; Jacobs et al., 2006; Wen et al., 2012), and forests (Berkelhammer et al., 2013; Dawson, 1998; Fritschen and Doraiswamy, 1973; Hiatt et al., 2012; Lai and Ehleringer, 2011). As compared to forests, grasslands present favorable conditions for dew and radiation fog formations: 1) Grassland surfaces are cooler than forest surfaces due to a higher albedo and thus lower net solar radiation input (Moore, 1976), and higher evapotranspiration (Kelliher et al., 1993; Williams et al., 2012). 2) Canopy resistance of grasslands is lower which reduces the warming effect by ground thermal emission via evaporative cooling (Garratt, 1992). 3) Aerosol particle deposition is weaker over grasslands due to shorter roughness length of grasslands (Gallagher et al., 2002), and thus more aerosol particles remain in the near-surface atmosphere, which consequently results in better conditions for radiation fog formation over grasslands. From the perspective of ecological functions, small amounts of NRW inputs have a more important influence on grasslands than forests because of the lower water use efficiency (hereafter WUE) and lower soil moisture availability in grasslands. At the beginning of drought stress in ecosystems, forests increase their WUE by closing their stomata, which increases stomatal resistance and thus reduces evapotranspiration, while grasslands maintain their evapotranspiration as long as the soil moisture is available to supply evaporative demand (e.g., Wolf et al. (2013)). Therefore, grasslands are more prone to suffer from soil water scarcity. In addition, as opposed to the deep-rooted systems for forest plants, grassland plants take up water from the top soil, where scarcity of soil moisture occurs more frequently during the absence of precipitation, therefore grasslands tend to anticipate lower soil moisture availability compared to forests.

Ambient water vapor is the main vapor source for both dew and radiation fog, therefore dew and radiation fog usually occur in combination. Because of the variability of temperature and humidity conditions, a single NRW night may transit from dew only to dew and radiation fog in combination. Before the atmospheric humidity reaches saturation, dew can only form if the surface temperature drops below air temperature. When the ambient water vapor reaches saturation or even super-saturation, dew and radiation fog can form in combination. Kaseke et al. (2017) used hydrogen and oxygen stable isotope regression to separate the different types of dew and fog, but they focused on dew and fog events separately. Research that focusses on relevant phase change processes during dew and radiation fog in combination is thus rare.

The moisture movement in the soil–plant–atmosphere continuum has been well understood by eddy covariance (hereafter EC) techniques, but the reliability of the method suffers during nighttime with weak turbulence (Berkelhammer et al., 2013). Instead, hydrogen and oxygen stable isotopes are a useful research tool to investigate different fractionation processes in the water cycle (Aemisegger et al., 2014; Delattre et al., 2015; Huang and Wen, 2014; Parkes et al., 2017), and can therefore be used to trace dew formation and radiation fog deposition into ecosystems (Delattre et al., 2015; He and Richards, 2015; Parkes et al., 2017; Spiegel et al., 2012; Wen et al., 2012). The isotopic composition of hydrogen (^{2}H and ^{1}H) or oxygen (^{18}O and ^{16}O) is expressed in the delta notation (hereafter δ) as $\delta = (R_{sample}/R_{standard} - 1) \cdot 1000$ ‰, where R_{sample} and $R_{standard}$ are the molar ratios of either ^{2}H/^{1}H or ^{18}O/^{16}O for the sample and standard, respectively. The standard is the Vienna Standard Mean Ocean Water (V-SMOW) controlled and distributed by the International Atomic Energy Agency (IAEA, 2009). With this definition, δ^{18}O and δ^2H are expressed as per mil (‰) discriminations from the standard. Whenever a phase change occurs, water molecules with different isotopes (hereafter isotopologue) as constituting atoms partition into the two phases in a specific way depending on ambient temperature and humidity gradients. Equilibrium fractionation always occurs at the interface between the two phases and results in a $\Delta\delta^2$H:$\Delta\delta^{18}$O ratio of approximately 8:1 in both phases, where Δ denotes the variabilities of δ^2H and δ^{18}O. When the ambient air is unsaturated, a deviation from the 8:1 ratio becomes measurable due to non-equilibrium fractionation (Dansgaard, 1964). The second order parameter deuterium excess (hereafter d), defined as $d = \delta^2\text{H} - 8\cdot\delta^{18}\text{O}$ after Dansgaard (1964), is a useful measure of non-equilibrium fractionation and provides information

https://doi.org/10.5194/hess-2020-493
Preprint. Discussion started: 13 October 2020

Hydrology and Earth System Sciences
Discussions

complementary to δ^2H and $\delta^{18}O$. The *d* is often used as a tracer for the water vapor source of a given water pool in the water cycle (Aemisegger et al., 2014; Galewsky et al., 2016; Gat, 1996; Welp et al., 2012; Yakir and Sternberg, 2000; Yepez et al., 2003). For example, at the local scale, local evaporation is a vapor source with lower *d*, while the entrainment from free troposphere is a vapor source with higher *d* (Delattre et al., 2015; Parkes et al., 2017). The diurnal cycle of deuterium excess in a well-mixed convective boundary layer has been studied previously (e.g., Lai and Ehleringer (2011)), whereas relevant processes affecting *d* in the NBL are much less well known, in particular for grasslands.

Monteith (1957) identified two input pathways for dew formation: 1) the downward pathway through the condensation of ambient water vapor onto foliage, and 2) the upward pathway through the condensation of soil-diffusing vapor onto foliage. Soil vapor diffusion is driven by the temperature gradient between the soil and the atmosphere and between different depths of the soil (Monteith, 1957; Oke, 1970). The temperature gradient generally reaches a maximum at the soil–atmosphere interface (2–4 °C warmer than the adjacent air at 1–2.5 cm in height for short grass or foliage surface (Monteith, 1957; Oke, 1970). The diffusing soil vapor can therefore condense onto cooler foliage. After Monteith (1957) had quantified the downward and upward components of dew formation by absorbing the NRW on foliage with filter paper, research has rarely been focusing on distinguishing these two pathways of dew formation. Furthermore, Monteith (1957) distinguished the two pathways by collecting the NRW in separate nights when only one or the other of the two pathways was assumed to occur. In Monteith (1957), the NRW condensing from soil-diffusing vapor was quantified in very calm nights with a 2 m wind speed (hereafter u_{2m}) of less than 0.5 m s^{-1}, whereas the maximum NRW condensing from ambient water was assumed to occur in slightly windy nights with u_{2m} in the range of 2–3 m s^{-1}. However, for clear calm nights with u_{2m} between 0.5 and 2 m s^{-1}, condensation of ambient water vapor and soil-diffusing vapor can occur in combination, with NRW on the foliage being a mix from these two pathways. Stable water isotopes and the "Keeling-plot" approach (Dawson, 1998; Keeling, 1958; Phillips et al., 2005) was used in this study to quantify the individual contributions of these two sources.

Our aim was to (1) investigate the isotopic fractionations during dew-only and dew–fog combined events; (2) estimate the potential gain of NRW from atmospheric vapor and from soil-diffusing vapor; and (3) assess the potential ecological relevance of NRW inputs to a temperate grassland ecosystem. We carried out three 24 h observation campaigns during summer 2018 using stable isotopes combined with EC and meteorological measurements to clarify the meteorological conditions and isotope fractionations for dew and radiation fog formations, to split the dew components from ambient water vapor and soil-diffusing vapor, and to explore the potential role of dew and radiation fog in temperate grasslands.

2 Materials and Methods

2.1 Study site and observation campaigns

The Chamau site (hereafter CH-CHA; 47°12′36.8″ N, 8°24′37.6″ E) is an intensively managed temperate grassland (4–6 cuts per year) at 393 m a.s.l., located in a valley bottom in Switzerland. The EC and meteorological measurement station (Fig. A1 in Appendix A) have been operational since 2005. The precipitation at the CH-CHA site was 870 mm in 2018, which was 297 mm (about 25%) less than the multiyear average over 2006–2017. From April to September in 2018, with respect to the corresponding monthly climatological values in the period 2006–2017, the monthly precipitation was on average 81 mm, which was averagely 49 mm (38%) less (Fig. 1a), and the monthly average temperature was on average 17.3 °C, which was 1.8 °C higher (Fig. 1b).

Three 24 h observation campaigns were carried out during expected dew/fog events on 25–26 July (event 1), 20–21 August (event 2), and 9–10 September (event 3) 2018. The time series were all recorded in CET (UTC+1). The corresponding consecutive no-rain periods were 23–27 July, 18–21 August, and 8–12 September 2018 respectively. Because of the extreme summer drought in 2018, no harvest of grassland was carried out during the three campaigns, but two harvests were carried out 46 d before event 1 on 9 June 2018, and one day after event 3 on 10 September 2018 respectively. The leaf area index

https://doi.org/10.5194/hess-2020-493
Preprint. Discussion started: 13 October 2020

Hydrology and Earth System Sciences
Discussions

(hereafter LAI) was 2.5 and 1.5 m^2 m^{-2} during events 1 and 2 respectively (measured 7 d before events 1 and 2 with LAI-2000, LI-COR Biosciences, Lincoln, NE, USA), and was 3.2 m^2 m^{-2} after harvest (measured 1 d after event 3). The mean vegetation height (z_c) was 0.2 – 0.3 m during the three campaigns. The volumetric soil water content at 10 cm was 18%, 18%, and 21% respectively (ML2x sensors, Delta-T Devices Ltd., Cambridge, UK). The permanent wilting point for the top soil at the site was 16% (calculated from soil texture at 0–20 cm: sand, 35.8%, clay, 19.0% following Roth (2006); the wilting point calculation equation followed Briggs and Shantz (1912)).

2.2 Experiment setup

2.2.1 Eddy covariance and meteorological data and calculations

The EC measurements at 20 Hz were setup at 2.4 m a.g.l. (see Zeeman et al. (2010) for more details), based on measurements with a 3-D sonic anemometer (Gill R3, Gill Instruments Ltd., Lymington, UK), and an open path Infrared Gas Analyzer (IRGA, Li-7500, Li-Cor, Lincoln, NE, USA). The EC measurements were processed to 30 min averages for evapotranspiration rate (mm h^{-1}), horizontal wind speed (hereafter u_{2m}, in m s^{-1}), H_2O flux (hereafter F_{H2O}, in mmol m^{-2} s^{-1}; minus value means downward flux, whilst positive value means upward flux), atmospheric specific humidity (hereafter q_a, in g kg^{-1}), and dew point temperature (hereafter T_d, in °C) (Buck, 1981; Campbell and Norman, 1998). The meteorological measurements at 0.1 Hz for air temperature (hereafter T_a, in °C), relative humidity (hereafter RH, in %), and long-wave outgoing radiation (hereafter LW_{out}, in W m^{-2}) were setup at 2.0 m a.g.l. (see Zeeman et al. (2010) and Fuchs et al. (2018) for more details). The horizontal visibility (in km) was measured every 10 s by a fog sensor (MiniOFS, Optical Sensors Inc., Goteborg, Sweden) and a present weather detector (PWD10, Vaisala Oyj, Helsinki, Finland). The meteorological measurements were processed to 30 min averages for T_a, RH, and LW_{out}, and to 1 min averages for visibility.

The vegetation surface temperature (T_0, in °C) was determined after Stefan–Boltzmann's law (Stull, 1988) as:

$$T_0 = \sqrt[4]{\frac{LW_{out}}{\varepsilon \cdot \sigma}} - 273.15\,, \tag{1}$$

where an emissivity (hereafter ε) of 0.98 was used to calculate temperatures for wet leaf surfaces (hereafter index w; $T_0 = T_{0w}$), and a value of 0.96 was used for dry leaf surfaces (hereafter index d $T_0 = T_{0d}$) after López et al. (2012); σ is Stefan-Boltzmann constant at $5.67 \cdot 10^{-8}$ W m^{-2} K^{-1}.

The saturation specific humidity (q_0, in g kg^{-1}) and the relative humidity (h_0) with respect to surface temperature T_0 for wet and dry vegetation surfaces was calculated using Tetens formula ((Buck, 1981; Campbell and Norman, 1998), see the equations in Appendix B).

2.2.2 Sampling of the NRW on foliage & isotope ratio mass spectrometer measurements

To analyze the isotopic compositions of the NRW on foliage, the NRW droplets were taken during dew and radiation fog formations. The sampling of the NRW on foliage (hereafter fNRW) was carried out on a grassland area of 100×130 m^2 around the "EC & meteo" measurements (Fig. A1 in Appendix A). Nine replicated fNRW samples were absorbed from leaf surfaces with cotton balls at the end of the nights of events 1 and 3 (once sampling per event), but bihourly during the night of event 2 (four times of sampling per event). After collection, the samples were immediately transferred into gas tight 12 ml exetainers (Labco Exetainer® vial, High Wycombe, UK) and stored in a portable cooling box filled with ice blocks. Before extracting the water in a cryogenic vacuum distillation system (Prechsl et al., 2015), the samples were stored at –19°C. The measurements of the isotopic compositions for fNRW (hereafter δ_{fNRW}) and in soil moisture (hereafter δ_s) of extracted water samples were performed using an isotope ratio mass spectrometer (IRMS, DELTAplusXP, Finnigan MAT, Bremen, Germany). The measured uncertainties of $\delta^{18}O$ and $\delta^{2}H$ are ±0.1‰ and better than ±1.0‰, respectively (Gehre et al., 2004; Werner and Brand, 2001).

https://doi.org/10.5194/hess-2020-493
Preprint. Discussion started: 13 October 2020

Hydrology and Earth System Sciences
Discussions

2.2.3 Isotopic compositions and mixing ratio measurements for ambient water vapor

The isotopic compositions and the volumetric mixing ratio for ambient water vapor were measured at 0.5–1 Hz using a cavity ring-down laser spectrometer (L2130-I, Picarro Inc., Santa Clara, CA, USA). The L2130-i was placed in a house 200 m away from the EC & meteo measurements (Fig. A1 in Appendix A). Ambient air was pulled into the L2130-i cavity through a PTFE intake hose, with an inner diameter of 1/4 inch, and a PTFE-filter inlet (FS-15-100 and TF50, Solberg International Ltd., Itasca, IL, USA) fixed at 6 m a.g.l.. The intake hose was thermally isolated, heated using a resistive heating wire (Raychem 5BTV2-CT, Von Rotz, Kerns, Switzerland) wrapped around the entire length of the intake tube to prevent condensation, and flushed with an external membrane pump (N022, KNF Neuberger GmbH, Munzingen, Freiburg, Germany) at a rate of 9 L min^{-1} to minimize memory effects within the inlet system. The isotopic compositions of ambient water vapor (hereafter δ_a) and the volumetric ambient water vapor mixing ratio (hereafter w) were measured with an instrumental flow rate of 300 mL min^{-1}. The instrument's response time in this setup was found to be on the order of 10 s Aemisegger et al. (2012).

To correct for instrument drifts and to normalize the data to the international VSMOW-SLAP scale, the raw data were calibrated using a Standard Delivery Module (SDM; A0101, Picarro Inc., Santa Clara, CA, USA) by performing two-point calibrations every 12 h (Aemisegger et al., 2012) using two liquid standards (standard 1: $\delta^{18}O_{s1}$ = –11.43‰, $\delta^{2}H_{s1}$ = –81.84‰, d_{s1} = 9.64‰; standard 2: $\delta^{18}O_{s2}$ = –40.66‰, $\delta^{2}H_{s2}$ = –325.67‰, d_{s2} = –0.37‰ measured by an IRMS). The $\delta^{18}O$ and $\delta^{2}H$ of the standards thus bracket the range of the measured $\delta^{18}O_a$ and $\delta^{2}H_a$. Laser spectrometric measurements are known to be affected by a water vapor mixing ratio dependent bias due to spectroscopic effects (absorption peak fitting, and baseline effects). In our study, all measurements were performed at w > 12 000 µmol mol^{-1}, therefore no mixing ratio dependent isotope bias correction was necessary (see more details in Aemisegger et al. (2012)). The L2130-i was calibrated using a dew point generator (LI-COR LI 610, Li-Cor Inc., Lincoln, NE, USA) following the procedure by Thurnherr et al. (2020).

The second-order parameter d of ambient water vapor (hereafter d_a) was calculated with the calibrated $\delta^{18}O_a$ and $\delta^{2}H_a$. The overall random uncertainties of $\delta^{18}O$ and $\delta^{2}H$ measurements were 0.2‰ and 0.8‰ respectively (for more details about the uncertainty quantification, see Aemisegger et al. (2012)). Calibrated $\delta^{18}O_a$ and $\delta^{2}H_a$ were then averaged over 30 min intervals.

To compare the ambient water vapor measurements with the fNRW, the NRW equilibrium liquid (aNRW) from this vapor was calculated. Under the assumption of equilibrium fractionation, the isotopic compositions of aNRW (hereafter δ_{aNRW}) formed from ambient water vapor (δ_a) were calculated using the temperature-dependent equilibrium fractionation factors following Horita and Wesolowski (1994) (see details in Appendix C).

2.3 Determination of atmospheric layer heights

The isotopic fractionation during phase change at the Earth surface is linked to the micrometeorological layers near the surface (Fig. 2). The inclusion of a zero-plane displacement (hereafter z-plane, Fig. 2) in wind profiles allows us to separate the downward flux from ambient water vapor and the upward flux from soil-diffusing vapor. The height of this z-plane (hereafter z_d, Fig. 2) is typically two-thirds of mean vegetation height (hereafter z_c, Fig. 2; Stull (1988)). The roughness length (hereafter z_0) is a measure of the aerodynamic roughness of the surface, and is around one-tenth of z_c (Fig. 2; Stull (1988)). The wind speed is zero at z_0 above z_d (z_d + z_0, Fig. 2; Stull (1988)). Therefore, we consider three pathways of NRW inputs onto the foliage of grasslands for dew and radiation fog: 1) the downward component of dew formation condensing from ambient water vapor (hereafter "aDew"), 2) the upward component of dew formation condensing from soil-diffusing vapor (hereafter "dDew"), and 3) radiation fog deposition (hereafter "aFog").

We determined the top of the NBL as the lowest height where the vertical stratification of the atmosphere becomes isothermal ($\partial T/\partial z$ = 0, Stull (1988); Tombrou et al. (1998)). During the three events in this study, the NBL top at 1:00 CET of the events was at 730 m, 700 m, and 680 m a.g.l., respectively (Fig. 3**)**; the NBL height was obtained from air pressure after Campbell and Norman (1998); the vertical temperature and pressure profiles were extracted from the hourly European Centre for Medium Range Weather Forecast (ECMWF) reanalysis product ERA5 reanalysis dataset within the Copernicus Climate

https://doi.org/10.5194/hess-2020-493
Preprint. Discussion started: 13 October 2020

Change Service (Hersbach et al., 2020; Horanyi, 2017). Canopy height z_c was 0.2–0.3 m during this time of season (Sect. 2.1), hence the aerodynamic displacement height z_d was roughly 0.13–0.20 m (≈2/3 z_c), with a roughness length z_0 of 0.02–0.03 m. With these assumptions, negligible wind speeds (u_{2m} around zero) could be assumed at heights below $z_d + z_0 \approx$ 0.15–0.23 m a.g.l. (Fig. 2).

2.4 Partitioning of NRW inputs using a two end-member mixing model

We split the contribution of NRW input pathways into the two main processes described in Sect. 2.3: (1) the downward component of dew formation (aDew) and fog droplet deposition (aFog), and (2) the distillation (dDew) of soil-diffusing vapor on plant leaves. In unsaturated conditions, the NRW on foliage (fNRW) was a mix of aDew and dDew, while in saturated conditions, fNRW was a mix of aDew and aFog. "Unsaturated conditions" in this context refers to the standard 2 m height of meteorological measurements. Both aDew and aFog were condensed from ambient water vapor, thus we used the term "aNRW" if either dew or fog input, or the combination of both, was meant. Dew formed in unsaturated conditions is a mixture of aNRW and dDew but lacks contribution from fog deposition, thus the isotopic signature of the NRW resulting from the isotopic compositions of dDew (hereafter $\delta^{18}O_{dDew}$ and $\delta^{2}H_{dDew}$) and the proportion of dDew (hereafter f_{dDew}) in fNRW was expressed as:

$$\delta^{18}O_{fNRW} = f_{dDew} \cdot \delta^{18}O_{dDew} + f_{aNRW} \cdot \delta^{18}O_{aNRW} , \quad (2)$$

$$\delta^{2}H_{fNRW} = f_{dDew} \cdot \delta^{2}H_{dDew} + f_{aNRW} \cdot \delta^{2}H_{aNRW} , \quad (3)$$

$$1 = f_{dDew} + f_{aNRW} , \quad (4)$$

where f_{aNRW} is the proportion of aNRW in fNRW; $\delta^{18}O_{dDew}$, $\delta^{2}H_{dDew}$, f_{dDew}, and f_{aNRW} are unknown. Therefore, four unknowns with only three equations (Eq. 2–4) required two time points, at 23:00 CET and 1:00 CET in event 2, to obtain empirical estimates for the four unknowns. By doing so, we implicitly assumed that $\delta^{18}O_{dDew}$ and $\delta^{2}H_{dDew}$ were constant within this 2 h period, and only f_{dDew} and f_{aNRW} were allowed to change between these two sampling times. For δ_{fNRW}, the median value for each sampling was taken, and for δ_{aNRW} the 2 h average was computed from 30 min data.

2.5 Statistics and imaging

In unspecified explicit, we reported means ± standard deviation. For δ_{fNRW} and d_{fNRW}, we reported median considering the heterogeneous distribution for the sampling of NRW on foliage. The calculating and imaging were processed in R version 3.6.3 (R Core Team, 2020). For linear regression between $\delta^{2}H$ and $\delta^{18}O$ the orthogonal regression was used (total least square, Gat (1981)), whereas the ordinary least-squares method was used for the d_a–RH and linear regression.

3 Results

3.1 Atmospheric and surface conditions during dew and radiation fog events

3.1.1 Weak turbulence and high relative humidity

Dew and radiation fog generally form during clear-sky nights with a weak large-scale pressure gradient, low wind speeds and weak turbulence. During the three field campaigns presented in this study, u_{2m} and F_{H2O} showed an abrupt weakening from around 17:00 CET onwards (Fig. 4a, b). With nightfall, u_{2m} remained below 0.7 m s^{-1} (Fig. 4a), and F_{H2O} was at very low (–0.4 to 0.3 mmol m^{-2} s^{-1}, minus value means downward flux, and positive value means upward flux; Fig. 4b), indicating a vanishing of turbulent fluxes. These are favorable conditions for dew and radiation fog formations.

The three events with dew or radiation fog were characterized by high relative humidity with respect to air temperature (RH) measured at 2 m above ground level. From around 17:00 CET, RH increased rapidly, and reached 100% around 03:00 CET during event 2, and around 20:30 CET during event 3 (Fig. 4c). These saturated conditions led to the formation of fog

https://doi.org/10.5194/hess-2020-493
Preprint. Discussion started: 13 October 2020


Hydrology and Earth System Sciences
Discussions

characterized by a horizontal visibility < 1 km (Fig. 4d). Fog appeared around 05:00 CET during event 2, lasting for less than an hour until sunrise, whilst the onset of fog was much earlier during event 3 (around 23:00 CET), lasting for a longer period until dissipation around sunrise. The visibility was always > 1 km in event 1, indicating that fog was absent during event 1. Therefore, event 1 can be considered as a dew-only event, whilst events 2 and 3 were characterized by a combination of dew and partial influence of radiation fog.

3.1.2 Surface cooling and the sign of condensation

Both grassland surfaces and ambient air started to cool down from around 17:00 CET onwards, due to substantial net long-wave radiation loss, which was not compensated by the low remaining incoming short-wave radiation levels. The leaf surfaces of the grassland cooled more rapidly than the near-surface atmosphere, thus with nightfall, T_0 remained cooler than T_a, although both of them gradually decreased (Fig. 5a). The first sign of condensation occurred when the leaf surfaces cooled down below dew point temperature (Fig. 5a, $T_0 < T_d$). The level of T_0 (T_{0d}) became lower than T_d at around 0:30 CET in event 1, 21:30 CET in event 2, and 19:00 CET in event 3 (Fig. 5a), determining when the first signs of condensation can be expected. During event 3, the surface already cooled down below the dew point rapidly after sunset ($T_0 < T_d$, Fig. 5a), indicating that condensation already started with nightfall.

The specific humidity of the air, q_a, steeply increased by 2.0–3.2 g kg^{-1} from around 17:00 CET until sunset (Fig. 5b), suggesting the inversion of moisture from local evaporation into a shallow inversion layer. The increase of q_a over time is enhanced by cold-air drainage down the slopes and along the valley bottom where the CH-CHA site is located as compared to conditions without advection. With nightfall, q_a reached a nighttime maximum of 9.6–12.5 g kg^{-1} (Fig. 5b). Especially, in events 1 and 2, before starting to decrease, q_a fluctuated for a short period from sunset until the first sign of condensation (Fig. 5b). When condensation started ($T_0 < T_d$, Fig. 5a), q_a gradually decreased (Fig. 5b). With q_0 falling to values below q_a (Fig. 5b), super-saturation with respect to the leaf surfaces occurred, thus computed theoretical h_0 exceeded 100% (Fig. 4c). The decrease of q_a was much faster in event 3 (0.4 g kg^{-1} h^{-1}, Fig. 5b) than that in events 1 and 2 (0.2 and 0.3 g kg^{-1} h^{-1}, Fig. 5b), indicating stronger condensation of ambient water vapor.

3.1.3 Characteristics of precondensation and condensation periods

According to the temperature and humidity conditions, the periods from 17:00 CET until sunrise were defined as: 1) precondensation period (hereafter P1) with the weakening of turbulence and with $T_0 > T_d$; and 2) condensation period (hereafter P2) with $T_0 < T_d$. The precondensation period (P1) was further separated into: P1a) starting around 17:00 CET until sunset with the weakening of turbulence and the increase of q_a; P1b) from sunset until the first sign of condensation with short-term fluctuations of q_a. The condensation period (P2) was further split into: P2a) with dew only under RH < 100%; P2b) with dew and radiation fog occurring in combination under RH = 100%.

3.2 Isotope dynamics of ambient water vapor during dew and fog events

The periods P1 and P2 are reflected in the temporal evolution of w, δ_a, and d_a (Fig. 6). During P1a as from 17:00 CET until sunset, w, $\delta^{18}O_a$, and δ^2H_a showed a steep increase by 0.3–0.4 mmol mol^{-1}, 2.0–3.2‰, and 7.4–12.5‰ respectively (Fig. 6a, b, c), whilst d_a showed a steep decrease by 11.6–16.9‰ (Fig. 6d). With nightfall when turning into period P1b, w and δ_a reached a plateau with 15.5 to 17.8 mmol mol^{-1} in w (Fig. 6a), –15.5 to –14.3‰ in $\delta^{18}O_a$ (Fig. 6b), and –128.0‰ to –113.2‰ in δ^2H_a (Fig. 6c). During P1b for events 1 and 2, w and δ_a experienced short-term fluctuations around their nighttime maximum before condensation set in, while d_a decreased by 5.1–9.4‰ (Fig. 6d). During P2, w steeply decreased by 0.8–5.5 mmol mol^{-1} (Fig. 6a), δ^2H_a decreased by 3.3–16.7‰ (Fig. 6c), and d_a reached its minimum at –11.8‰ to –4.7‰ (Fig. 6d). During P2, the decreasing rate of δ^2H_a in event 3 (1.6‰ δ^2H_a h^{-1}) was almost double of that in events 1 and 2 (0.8 and 1.0 δ^2H_a h^{-1} respectively, Fig. 6c), suggesting stronger condensation in event 3.

https://doi.org/10.5194/hess-2020-493
Preprint. Discussion started: 13 October 2020

Hydrology and Earth System Sciences
Discussions

Note that the changes of $\delta^{18}O_a$ and d_a (Fig. 6b, d) depended on the humidity dynamics and the occurrence of dew and fog (Fig. 4c, d). During the dew-only P2a in events 1 and 2 (Fig. 4c, d), δ^2H_a decreased by 3.3–5.7‰ (Fig. 6c), and d_a slightly decreased by 3.4–3.7‰ (Fig. 6d), while $\delta^{18}O$ showed slight fluctuations around the maximum reached 4 h and 2 h after nightfall of events 1 and 2 respectively (–15.5‰ to –14.3‰, Fig. 6b). During P2b in events 2 and 3 with dew and fog in combination, both $\delta^{18}O_a$ and δ^2H_a gradually decreased (by 0.3–1.5‰, and 2.1–12.8‰ respectively) with a ratio of around 8:1 (Fig. 6b, c), hence d_a was approximately constant at the nighttime minimum (–6.0‰ to –4.7‰, Fig. 6d) although with slight fluctuation.

3.3 The isotopic signals of non-rainfall water

The NRW on foliage (fNRW) was comparable with the equilibrium liquids from ambient water vapor (aNRW). The isotopic compositions of aNRW was –5.0‰ to –4.3‰ in $\delta^{18}O_{aNRW}$, –47.4‰ to –38.6‰ in δ^2H_{aNRW}, and –12.1‰ to –2.4‰ in d_{aNRW} (Fig. 7a, b, c). As a comparison, the NRW on foliage (fNRW) was –6.1‰ to –1.5‰ in $\delta^{18}O_{fNRW}$, –64.3‰ to –35.6‰ in δ^2H_{fNRW}, and –33.8‰ to 8.0‰ in d_{fNRW} (Fig. 7a, b, c). The isotopic compositions of fNRW varied in time with gradually decreasing $\delta^{18}O_{fNRW}$ (Fig. 7a), but gradually increasing δ^2H_{fNRW} (Fig. 7b) and d_{fNRW} (Fig. 7c).

The relationships between the isotopic compositions of fNRW and aNRW were related to RH. Under unsaturated conditions during P2a when dew formation occurred, $\delta^{18}O_{aNRW}$ (–4.4±0.1‰) was more depleted than $\delta^{18}O_{fNRW}$ (–3.8‰) (Fig. 7a), while δ^2H_{aNRW} (–42.3±3.8‰) was more enriched than δ^2H_{fNRW} (–47.7‰) (Fig. 7b), and d_{aNRW} (–7.1±3.6‰) was higher than d_{fNRW} (–20.5‰) (Fig. 7c). Under saturated conditions during P2b, the isotopic compositions of aNRW (–4.7±0.2‰ in $\delta^{18}O_{aNRW}$, –43.0±1.2‰ in δ^2H_{aNRW}, and –5.4±0.3‰ in d_{aNRW}) was identical to the isotopic compositions of fNRW (–4.6‰ in $\delta^{18}O_{fNRW}$, –41.6‰ in δ^2H_{fNRW}, and –4.7‰ in d_{fNRW}) (Fig. 7a, b, c). Especially, for the sampling at 5:00 CET in event 3 when radiation fog occurred, $\delta^{18}O_{fNRW}$ and δ^2H_{fNRW} were depleted by 0.7‰ and 1.4‰ with respect to $\delta^{18}O_{aNRW}$ and δ^2H_{aNRW} respectively (Fig. 7a, b), and d_{aNRW} was 5.5‰ higher than d_{fNRW} (Fig. 7c).

The relationships of δ^2H_{fNRW}–$\delta^{18}O_{fNRW}$ and δ^2H_{aNRW}–$\delta^{18}O_{aNRW}$ with respect to the local meteorological water line (LMWL: $\delta^2H = 7.68 \times \delta^{18}O + 6.97$, Prechsl et al. (2014)) were shown in Fig. 8. Both δ^2H_{fNRW}–$\delta^{18}O_{fNRW}$ and δ^2H_{aNRW}–$\delta^{18}O_{aNRW}$ fell to the right side of LMWL, suggesting lower d from NRW inputs as compared to local precipitation. When we only considered the condensation of ambient water vapor under equilibrium fractionation, δ^2H_{fNRW} and $\delta^{18}O_{fNRW}$ distributed on the equilibrium line (orthogonal regression) from δ^2H_{aNRW}–$\delta^{18}O_{aNRW}$ (for the sampling at 3:00 and 5:00 CET in event 2, Fig. 8). However, with the mix of the component condensing from soil-diffusing vapor (dDew) under RH < 100%, the δ^2H_{fNRW}–$\delta^{18}O_{fNRW}$ pairs fell to the right-hand side of the equilibrium line (for the sampling at 3:00 CET in event 1, and the samplings at 23:00 and 1:00 in event 2, Fig. 8a), suggesting lower d_{fNRW} than d_{aNRW}. Whereas, with the mix of the component from radiation fog deposition, δ^2H_{fNRW}–$\delta^{18}O_{fNRW}$ relation fell to the left-hand sides of the equilibrium line (for the sampling at 5:00 CET in event 3), indicating higher d_{fNRW} than d_{aNRW}.

3.4 Splitting the components of dew using a two end-member mixing model

Under unsaturated conditions, with respect to aNRW, $\delta^{18}O_{fNRW}$ and δ^2H_{fNRW} deviated to the enriched and depleted sides of $\delta^{18}O_{aNRW}$ and δ^2H_{aNRW}, respectively (Fig. 7a, b), suggesting a mix of NRW on foliage (fNRW) from the condensation of soil-diffusing vapor (dDew) and the condensation of ambient water vapor (aNRW). Based on the measurements from 23:00 to 1:00 CET in event 2, the averages of $\delta^{18}O_{dDew}$, δ^2H_{dDew}, and d_{dDew} during this 2 h period were estimated as –1.0‰, –71.8‰, and –63.4‰ respectively (Fig. 7a, b, c), and the corresponding contributions of dDew in fNRW were 28% and 9% respectively (Fig. 7d). A linear extrapolation from the two hours between 23:00 CET and 1:00 CET to the beginning of dew formation at 21:30 CET of event 2 increased the contribution of dDew to 42% (Fig. 7d). Similarly, when using the values of δ_{dDew} from event 2 for estimating the contribution of dDew during event 1, the proportion of dDew was around 18–31% for our sampling at 3:00 CET of event 1 (vertical whiskers in Fig. 7d).

https://doi.org/10.5194/hess-2020-493
Preprint. Discussion started: 13 October 2020

Hydrology and Earth System Sciences
Discussions

4 Discussion

4.1 Fractionation during condensation of ambient water vapor

We only considered equilibrium fractionation (shown as δ_{aNRW} in Fig. 9) when simulating the isotopic compositions of the NRW component condensing from ambient water vapor. An alternative approach would be to consider both equilibrium and non-equilibrium fractionation factors (see Appendix D; see also Lee et al. (2009) and Wen et al. (2012)) because of the laminar sublayer in the leaf boundary layer. To compare these two methods, we applied the method of Wen et al. (2012) on our data to simulate the isotopic composition of the NRW component condensing from ambient water vapor (shown as δ_{naNRW} in Fig. 9; see also Appendix D). We found that δ_{naNRW} was more depleted as compared to the NRW on foliage (shown as δ_{fNRW} in Fig. 9), and the depletion of δ_{naNRW} was more severe with the increase of h_0 (Fig. 4c), which is in agreement with Wen et al. (2012). The depletion of δ_{naNRW} with respect to δ_{fNRW} was most likely due to the overestimation of the non-equilibrium fractionation factor when h_0 exceeded 100% (going up to 132% in our study, see Fig. 4c), because Jouzel et al. (1987) pointed out that non-equilibrium fractionation is negligible above –10 °C in the process of vapor condensing to liquid. However, non-equilibrium fractionation driven by molecular diffusion might have played an important role in a laminar fog boundary layer (hereafter FBL; (Castillo and Rosner, 1989; Epstein et al., 1992)), which led to more depleted δ_{fNRW} than δ_{aNRW} at 5:00 CET in event 3 (Fig. 7a, b) when radiation fog occurred. Heavier isotopologues move more slowly than their lighter counterpart in air (molecular diffusivity: $D[^1H_2{}^{18}O] < D[^1H^2H^{16}O] < D[^1H_2{}^{16}O]$, Merlivat (1978)), hence the rate at which heavy isotopologues ($^1H_2{}^{18}O$ and $^1H^2H^{16}O$) in ambient air pass through the laminar FBL to be condensed at the liquid–vapor interface is smaller than the rate of condensation of their lighter counterpart. Therefore, δ_{fNRW} can become more depleted than δ_{aNRW}. Fog lasted as from 23:00 CET until sunrise of event 3, and appeared around 5:00 CET within half an hour before sunrise in event 2 (Fig. 4d). However, we only observed a lower δ_{fNRW} than δ_{aNRW} in event 3 (Fig. 7a, b), suggesting that the depletion of δ_{fNRW} might also be related to the duration of radiation fog. The condensation of ambient water vapor for dew formation can be approximated as an equilibrium fractionation process accordingly, as was also observed by Wen et al. (2012) and Delattre et al. (2015). The condensation of ambient water vapor to form radiation fog can cause slight depletion of the NRW compared to the equilibrium liquid obtained from ambient water vapor.

4.2 Potential NRW gain from the condensation of soil-diffusing vapor

Splitting the input pathways of dew formation using stable isotopes will allow future studies to quantify dDew gain with the combination of lysimetric or filter paper absorption measurements. In our study, as shown in Sect. 3.4, we estimated that dDew contributed 9–42% of total NRW (Fig. 7d) during our observation periods. Monteith (1957) estimated that the condensation rate of soil-diffusing vapor was 0.01–0.02 mm h^{-1} (with u_{2m} < 0.5 m s^{-1}) using filter paper absorption measurements. In Monteith (1957), the condensation rate of ambient water vapor varied from 0.004 to 0.035 mm h^{-1} depending on the wind speed (with u_{2m} < 3 m s^{-1}) and humidity conditions. Thus, the contribution of dDew in the total NRW was potentially 22–83 % according to the condensation rate of Monteith (1957). Following the condensation rate of Monteith (1957), the potential total NRW gain was 0.06 – 0.39 mm $night^{-1}$ (see details in Table 2). This amount of NRW gain was comparable with the average evapotranspiration rate of 2.8 mm day^{-1} (daytime) during the continuous no-rain periods of the three events (see details in Table 3).

In future research, combining isotopic compositions measurements with lysimetric measurements to quantify dDew gain would provide useful benchmark data to better evaluate the isotope-based estimates of NRW input. The NRW gain can be measured directly by a lysimeter as the net water gain of the soil and plants (Kaseke et al., 2012; Riedl et al., 2020; Ucles et al., 2013), while dDew is an indirect estimate based on stable water isotope data of the transfer of moisture from one part of the surface (soil surface) to another (foliage) within grassland ecosystems.

https://doi.org/10.5194/hess-2020-493
Preprint. Discussion started: 13 October 2020


Hydrology and Earth System Sciences
Discussions

4.3 Diurnal patterns of isotopic compositions in ambient water vapor

The diurnal patterns of d_a reflected the main drivers of ambient moisture variability. During the daytime 13:00–17:00 CET, d_a was at a plateau (12.2‰ to 18.0‰, Fig. 6d) compared to condensation periods in the night (P2), when d_a reached its daily minimum (–11.8‰ to –4.7‰, Fig. 6d). The transition from higher daytime d_a to lower nighttime d_a occurred from 17:00 CET until sunset (P1a, Fig. 6d). Entrainment from the free troposphere played a dominant role in daytime atmospheric moisture during 13:00–17:00 CET, and caused a higher d_a than in the night (Fig. 6d), and a decrease in δ_a (Fig. 6b, c) (Delattre et al., 2015; Lai et al., 2006; Lee et al., 2006; Parkes et al., 2017; Welp et al., 2012). On the contrary, during P1a, under reduced entrainment from the free troposphere (weakened u_{2m}, and reduced F_{H2O} in Fig. 4a, b) compared to mid-day values, local ET caused a steep decrease of d_a (Fig. 6d) and increases of δ_a (Fig. 6b, c), which was in accordance with the previous research by Lai et al. (2006), Huang and Wen (2014), and Parkes et al. (2017). During P1b, the fluctuation of δ_a (Fig. 6b, c) was due to short-term variability of the isotopic compositions of soil evaporation (within 1 h before sunset, 0–5 cm soil moisture with $\delta^{18}O$ varying from 5.5‰ to –8.5‰, with $\delta^{2}H$ varying from –8.5‰ to –72.8‰, and d varying from –5.0‰ to –52.4‰), which was in accordance with the reports by Welp et al. (2012). The decrease of δ_a during P2b suggested radiation fog with local moisture as a source for ambient water vapor, which was in contrast with Spiegel et al. (2012) in Greenland that found the increase of δ_a with fog during the passage of a cold front. The correlated d_a – T_a (Fig. 10a) and anti-correlated d_a–RH (Fig. 10b) in our study suggested an only minor influence of large-scale air advection and highlighted the dominant role of local moisture as a source for ambient water vapor (Aemisegger et al., 2014).

During dew and radiation fog (P2), the condensation of ambient water vapor could essentially be described by an equilibrium fractionation process, with d_a remained constant at a low nighttime minimum level (Fig. 6d) (Delattre et al., 2015; Huang and Wen, 2014). However, soil evaporation occurred synchronously with condensation. Soil evaporation in saturated ambient air (RH = 100 % at 2 m a.g.l.) is essentially an equilibrium fractionation process (Eichinger et al., 1996; Priestley and Taylor, 1972), which did not affect the variability of d_a during P2b (Fig. 6d). Whereas, non-equilibrium fractionation is intrinsically dominant in the processes of soil evaporation in unsaturated ambient air (RH < 100 % at 2 m a.g.l.), which induced a slight d_a decrease during P2a (Fig. 6d). In addition, cold air drainage along the valley to the bottom where the CH-CHA site is located (Eugster and Merbold, 2015), might have enhanced the effect of local soil evaporation on δ_a variability.

4.4 Ecological functions of non-rainfall water

From the perspective of ecological functions, dDew might be more important than previously thought, although it has no large-scale hydrological significance of moisture transfer from one part of the surface to another (Monteith, 1957). This can be expected if the transfer of moisture is from a hydrological pool that is inaccessible to plants (e.g., soil-diffusing vapor) to another that is accessible to plants (e.g., droplets forming or depositing on leaf surfaces or on the surface soil where it can be accessed by the fine roots). The condensation of soil-diffusing vapor was comparable with the condensation of ambient water vapor in our study (contributing 9–42% during our observation periods, Fig. 7d), and was the dominant pathway of NRW inputs during very calm night (u < 0.7 m s^{-1}; see also Monteith (1957)) when the flux from ambient air to the grassland surface was very small. Soil vapor diffusion occurs as long as a temperature gradient exists (see the soil temperature at different depths in Fig. E1 of Appendix E), which results in vapor pressure differences along that gradient. Therefore, soil vapor diffusion transfers the deeper soil vapor to the surface, from where it moistens the air in contact with the soil surface. Subsequently, this moisture condenses onto foliage and becomes available to the plants. Wang et al. (2017) observed that 0.0092 mm of water were transferred from deeper soil layers to the surface by vapor diffusion in a grassland plot, although it was doubtful whether the water went onto foliage or was absorbed by the top soil. The soil diffusion rate increases with the decrease of soil water content (under volumetric soil moisture content higher than 10% (Barnes and Turner, 1998; Philip and De Vries, 1957)), which makes soil vapor diffusion more important in conditions of low soil moisture. The NRW inputs for dew and radiation fog are expected to be taken up by plants through foliar water uptake or be dripping down to wet the soil surface, thereby potentially

https://doi.org/10.5194/hess-2020-493
Preprint. Discussion started: 13 October 2020

preventing permanent damage of the plants by drought stress (e.g., Schreel and Steppe (2020)). The ecological functions of NRW was also reflected in its thermal effect on the plants. The leaf wetting by NRW which potentially cooled the leaf surfaces by 1.5 °C in comparison to dry leaf surfaces (differences between T_{0w} and T_{0d}, Fig. 5a), thereby alleviating potential plant heat stress during the early morning hours when solar radiation quickly increases after sunrise.

Further research should thus focus on the plant water status in response to NRW inputs from dew and radiation fog. In addition, future research focusing on the continuous measurement of the isotopic compositions ($\delta^{18}O$ and $\delta^{2}H$) of soil vapor would give more quantitative insights on vapor transfer in soils during dew and radiation fog nights. The condensation of soil-diffusing vapor is expected to play a more important role in temperate grasslands than in arid grasslands, if soil salinity and canopy resistance are also taken into consideration: Soil salinity reduces the rate of soil vapor diffusion (Gran et al., 2011). In a laminar boundary layer during dew and radiation fog events, dense canopies in temperate grasslands (LAI was 1.5–3.2 m^2 m^{-2} for summer 2018 at the CH-CHA site, Sect. 2.1) potentially shield the uppermost soil vapor from being exported into the near-surface atmosphere, while sparse canopies in arid grasslands (LAI around 0.5 m^2 m^{-2} as e.g. in Wen et al. (2012)) should result in most of the soil-diffusing vapor being emitted into the atmosphere.

5 Conclusion

Our results reveal different input pathways for dew and radiation fog in a temperate grassland during three dry intensive observation periods in summer 2018 in Switzerland. Dew and radiation fog occurred in clear calm nights with very low wind speed ($u < 0.7$ m s^{-1}) and weak turbulence with near-zero net water vapor flux at the vegetation surface (F_{H2O} at –0.4 to 0.3 mmol m^{-2} s^{-1}). Condensation of ambient water vapor during dew and radiation fog was found to be predominantly an equilibrium fractionation process, which was deduced from the rather constant d_a during NRW nights. This caused a decrease of 0.8–1.6‰ $\delta^{2}H_a$ h^{-1} in ambient water vapor during dew and radiation fog. In unsaturated conditions (determined at the meteorological 2 m reference height), condensation occurred from ambient air above the canopy as well as soil-diffusing vapor below the canopy, as was indicated by a 3.4–3.7‰ decrease of d_a. Local evaporation at high relative humidity from 17:00 CET until sunset caused the lowering of d_a to values in the range of 2.4‰ to 4.8‰ as compared to the higher daytime d_a (12.2‰ to 18.0‰). A further decrease to d_a values in the range of –11.8‰ to –4.7‰ was observed during the occurrence of dew and radiation fog at night. Dew only formed under unsaturated conditions with a mixed NRW condensing from ambient water vapor and soil-diffusing vapor. The comparison between the foliage NRW δ_{fNRW} and the equilibrium NRW δ_{aNRW} of ambient water vapor allowed us to trace the source of the NRW input pathways during dew formation. The NRW condensing from soil-diffusing vapor contributed 9–42% of the foliage NRW. The correlated $d_a - T_a$ and anti-correlated d_a–RH suggested an only minor influence of large-scale air advection and highlighted the dominant role of local moisture as a source for ambient water vapor.

In future studies, continuous isotope measurements of foliage NRW, ambient water vapor and soil vapor should be combined with direct lysimetric and filter paper absorption measurements, as well as physiological measurements to more precisely quantify the NRW input pathways, and the mechanisms of plant water status responding to NRW input on foliage. Confirmation of dew and radiation fog inputs into temperate ecosystems during summer drought by the isotopic compositions of NRW and ambient water vapor would then allow assessing the potential response of these ecosystems to warming and increased frequency of summer droughts under the global climate changes.

The dew and radiation fog potentially produced 0.06–0.39 mm $night^{-1}$ NRW gain on foliage, which was comparable with 2.8 mm day^{-1} daytime evapotranspiration. With increasing relative humidity, the share of vapor originating from soil vapor diffusion decreased, whereas the relevance of atmospheric water vapor for dew formation increased. This atmospheric water vapor had a rather local isotopic signature, which suggests that large-scale moisture advection only has a minor influence in the nocturnal NRW gains during dew and radiation fog events. Our results thus highlight the importance of NRW inputs to

https://doi.org/10.5194/hess-2020-493
Preprint. Discussion started: 13 October 2020

temperate grasslands during prolonged dry periods and reveal the complexity of the local water cycle in such conditions including different pathways of water deposition.

6 Data availability

Data will be deposited at the ETH Zurich research collection at https://doi.org/10.3929/ethz-b-000445289.

Author contributions. YL, AR, WE, and FA designed the project. YL and AR performed the field experiment. YL carried out the laboratory work. YL performed all statistical analyses. FA wrote the code of data calibration for the ambient water vapor isotopes. FA and WE commented on the results of the data analysis. YL wrote and revised the manuscript, with contributions and feedbacks by FA, WE, AR, and NB.

Acknowledgements. This study was supported by Swiss National Science Foundation (grant 175733, IFDewS project). The Picarro L2130-i analyser was provided by the Atmospheric Dynamics group (Prof. Heini Wernli) at ETH Zurich. We thank Iris Feigenwinter, ETH Zurich, for the quality check of EC and meteorological data as well as measurements of LAI, and Kathrin Fuchs, KIT Garmisch-Partenkirchen (Germany), for her introduction to the Chamau (CH-CHA) field site. The Canton of Zug staff maintaining the agricultural management of the Chamau field site are thanked for their support. The authors also acknowledge MeteoSwiss and ECWMF for the access to the ERA5 reanalysis data products.

References

Aemisegger, F., Pfahl, S., Sodemann, H., Lehner, I., Seneviratne, S. I., and Wernli, H.: Deuterium excess as a proxy for continental moisture recycling and plant transpiration, Atmospheric Chemistry and Physics, 14, 4029-4054, https://doi.org/10.5194/acp-14-4029-2014, 2014.

Aemisegger, F., Sturm, P., Graf, P., Sodemann, H., Pfahl, S., Knohl, A., and Wernli, H.: Measuring variations of $\delta^{18}O$ and $\delta^{2}H$ in atmospheric water vapour using two commercial laser-based spectrometers: an instrument characterisation study, Atmos. Meas. Tech., 5, 1491-1511, https://doi.org/10.5194/amt-5-1491-2012, 2012.

Agam, N. and Berliner, P. R.: Dew formation and water vapor adsorption in semi-arid environments - A review, Journal of Arid Environments, 65, 572-590, https://doi.org/10.1016/j.jaridenv.2005.09.004, 2006.

Atzema, A. J., Jacobs, A. F. G., and Wartena, L.: Moisture distribution within a maize crop due to dew, Netherlands Journal of Agricultural Science, 38, 117-129, https://doi.org/10.18174/njas.v38i2.16599, 1990.

Barnes, C. J. and Turner, J. V.: Chapter 5 - Isotopic Exchange in Soil Water, in: Isotope Tracers in Catchment Hydrology, edited by: Kendall, C. and McDonnell, J. J., Elsevier, Amsterdam, 137-163, https://doi.org/10.1016/B978-0-444-81546-0.50012-4, 1998.

Berkelhammer, M., Hu, J., Bailey, A., Noone, D. C., Still, C. J., Barnard, H., Gochis, D., Hsiao, G. S., Rahn, T., and Turnipseed, A.: The nocturnal water cycle in an open-canopy forest, Journal of Geophysical Research-Atmospheres, 118, 10225-10242, https://doi.org/10.1002/jgrd.50701, 2013.

Beysens, D., Clus, O., Mileta, M., Milimouk, I., Muselli, M., and Nikolayev, V. S.: Collecting dew as a water source on small islands: the dew equipment for water project in Bisevo (Croatia), Energy, 32, 1032-1037, https://doi.org/10.1016/j.energy.2006.09.021, 2007.

Briggs, L. J. and Shantz, H. L.: The wilting coefficient and its indirect determination, Bot Gaz, 53, 0020-0037, https://www.jstor.org/stable/2467365, 1912.

Buck, A. L.: New Equations for Computing Vapor Pressure and Enhancement Factor, Journal of Applied Meteorology, 20, 1527-1532, https://doi.org/10.1175/1520-0450(1981)020%3C1527:NEFCVP%3E2.0.CO;2, 1981.

Campbell, G. S. and Norman, J. M.: Water Vapor and Other Gases, in: An Introduction to Environmental Biophysics, edited by: Campbell, G. S. and Norman, J. M., Springer New York, New York, NY, 37-51, https://doi.org/10.1007/978-1-4612-1626-1_3, 1998.

Castillo, J. L. and Rosner, D. E.: Theory of Surface Deposition from a Unary Dilute Vapor-Containing Stream Allowing for Condensation within the Laminar Boundary-Layer, Chem Eng Sci, 44, 925-937, https://doi.org/10.1016/0301-9322(89)90088-8, 1989.

Clus, O., Ortega, P., Muselli, M., Milimouk, I., and Beysens, D.: Study of dew water collection in humid tropical islands, Journal of Hydrology, 361, 159-171, https://doi.org/10.1016/j.jhydrol.2008.07.038, 2008.

Dansgaard, W.: Stable isotopes in precipitation, Tellus, 16, 436-468, https://doi.org/10.1111/j.2153-3490.1964.tb00181.x, 1964.

Dawson, T. E.: Fog in the California redwood forest: ecosystem inputs and use by plants, Oecologia, 117, 476-485, https://doi.org/10.1007/s004420050683, 1998.

del Prado, R. and Sancho, L. G.: Dew as a key factor for the distribution pattern of the lichen species Teloschistes lacunosus in the Tabernas Desert (Spain), Flora, 202, 417-428, https://doi.org/10.1016/j.flora.2006.07.007, 2007.

Delattre, H., Vallet-Coulomb, C., and Sonzogni, C.: Deuterium excess in the atmospheric water vapour of a Mediterranean coastal wetland: regional vs. local signatures, Atmos. Chem. Phys., 15, 10167-10181, https://doi.org/10.5194/acp-15-10167-2015, 2015.

Dongmann, G., Nurnberg, H. W., Forstel, H., and Wagener, K.: On the enrichment of $H_2^{18}O$ in the leaves of transpiring plants, Radiation and Environmental Biophysics, 11, 41-52, https://doi.org/10.1007/BF01323099, 1974.

Eichinger, W. E., Parlange, M. B., and Stricker, H.: On the concept of equilibrium evaporation and the value of the Priestley-Taylor coefficient, Water Resources Research, 32, 161-164, https://doi.org/10.1029/95WR02920, 1996.

Epstein, M., Hauser, G. M., Fauske, H. K., Grolmes, M. A., Henry, R. E., and Leung, J. C.: Fog Formation and Deposition within Laminar and Turbulent Natural-Convection Boundary-Layers Along Cold Vertical Plates, Chem Eng Commun, 118, 163-187, https://doi.org/10.1080/00986449208936092, 1992.

Eugster, W. and Merbold, L.: Eddy covariance for quantifying trace gas fluxes from soils, Soil, 1, 187-205, https://doi.org/10.5194/soil-1-187-2015, 2015.

Fritschen, L. J. and Doraiswamy, P.: Dew - An dddition of hydrologic balance of Douglas -Fir, Water Resources Research, 9, 891-894, https://doi.org/10.1029/WR009i004p00891, 1973.

Fuchs, K., Hörtnagl, L., Buchmann, N., Eugster, W., Snow, V., and Merbold, L.: Management matters: testing a mitigation strategy for nitrous oxide emissions using legumes on intensively managed grassland, Biogeosciences, 15, 5519-5543, https://doi.org/10.5194/bg-15-5519-2018, 2018.

Galewsky, J., Steen-Larsen, H. C., Field, R. D., Worden, J., Risi, C., and Schneider, M.: Stable isotopes in atmospheric water vapor and applications to the hydrologic cycle, Reviews of Geophysics, 54, 809-865, https://doi.org/10.1002/2015RG000512, 2016.

Gallagher, M. W., Nemitz, E., Dorsey, J. R., Fowler, D., Sutton, M. A., Flynn, M., and Duyzer, J.: Measurements and parameterizations of small aerosol deposition velocities to grassland, arable crops, and forest: Influence of surface roughness length on deposition, Journal of Geophysical Research-Atmospheres, 107, https://doi.org/10.1029/2001JD000817, 2002.

Garratt, J. R.: The atmospheric boundary layer, Earth-Science Reviews, 1-2, Cambridge University Press, 89-134 pp., 1992.

Gat, J. R.: Oxygen and hydrogen isotopes in the hydrological cycle, Annual Review of Earth and Planetary Sciences, 24, 225-262, https://doi.org/10.1146/annurev.earth.24.1.225, 1996.

Gat, J. R.: Stable isotope hydrology Deuterium and oxygen-18 in the water cycle, IAEA, International Atomic Energy Agency (IAEA), https://inis.iaea.org/collection/NCLCollectionStore/_Public/13/677/13677657.pdf?r=1, 1981.

Gehre, M., Geilmann, H., Richter, J., Werner, R. A., and Brand, W. A.: Continuous flow $^{2}H/^{1}H$ and $^{18}O/^{16}O$ analysis of water samples with dual inlet precision, Rapid communications in mass spectrometry, 18, 2650-2660, https://doi.org/10.1002/rcm.1672, 2004.

Gran, M., Carrera, J., Massana, J., Saaltink, M. W., Olivella, S., Ayora, C., and Lloret, A.: Dynamics of water vapor flux and water separation processes during evaporation from a salty dry soil, Journal of Hydrology, 396, 215-220, https://doi.org/10.1016/j.jhydrol.2010.11.011, 2011.

He, S. and Richards, K.: The role of dew in the monsoon season assessed via stable isotopes in an alpine meadow in Northern Tibet, Atmospheric Research, 151, 101-109, https://doi.org/10.1016/j.atmosres.2014.02.014, 2015.

Hersbach, H., Bell, B., Berrisford, P., Hirahara, S., Horanyi, A., Munoz-Sabater, J., Nicolas, J., Peubey, C., Radu, R., Schepers, D., Simmons, A., Soci, C., Abdalla, S., Abellan, X., Balsamo, G., Bechtold, P., Biavati, G., Bidlot, J., Bonavita, M., De Chiara, G., Dahlgren, P., Dee, D., Diamantakis, M., Dragani, R., Flemming, J., Forbes, R., Fuentes, M., Geer, A., Haimberger, L., Healy, S., Hogan, R. J., Holm, E., Janiskova, M., Keeley, S., Laloyaux, P., Lopez, P., Lupu, C., Radnoti, G., de Rosnay, P., Rozum, I., Vamborg, F., Villaume, S., and Thepaut, J. N.: The ERA5 global reanalysis, Quarterly Journal of the Royal Meteorological Society, 146, 1999-2049, https://doi.org/10.1002/qj.3803, 2020.

Hiatt, C., Fernandez, D., and Potter, C.: Measurements of fog water deposition on the California central coast, Atmospheric and Climate Sciences, 2, 525-531, http://dx.doi.org/10.4236/acs.2012.24047, 2012.

Horanyi, A.: Some aspects on the use and impact of observations in the ERA5 Copernicus Climate Change Service reanalysis, Idojaras, 121, 329-344, 2017.

Horita, J. and Wesolowski, D. J.: Liquid-vapor fractionation of oxygen and hydrogen isotopes of water from the freezing to the critical temperature, Geochimica et Cosmochimica Acta, 58, 3425-3437, https://doi.org/10.1016/0016-7037(94)90096-5, 1994.

Huang, L. and Wen, X.: Temporal variations of atmospheric water vapor δD and $\delta^{18}O$ above an arid artificial oasis cropland in the Heihe River Basin, Journal of Geophysical Research: Atmospheres, 119, 11,456-411,476, https://doi.org/10.1002/2014JD021891, 2014.

IAEA: Reference Sheet for VSMOW2 and SLAP2 International Measurement Standards, International Atomic Energy Agency (IAEA), Vienna, Austria, 8 pp., 2009.

Jacobs, A. F. G., Heusinkveld, B. G., and Berkowicz, S. M.: A simple model for potential dewfall in an arid region, Atmospheric Research, 64, 285-295, https://doi.org/10.1016/S0169-8095(02)00099-6, 2002.

Jacobs, A. F. G., Heusinkveld, B. G., Kruit, R. J. W., and Berkowicz, S. M.: Contribution of dew to the water budget of a grassland area in the Netherlands, Water Resources Research, 42, https://doi.org/10.1029/2005WR004055, 2006.

Jouzel, J., Russell, G. L., Suozzo, R. J., Koster, R. D., White, J. W. C., and Broecker, W. S.: Simulations of the HDO and $H_2{}^{18}O$ atmospheric cycles using the NASA GISS general circulation model: The seasonal cycle for present-day conditions, Journal of Geophysical Research: Atmospheres, 92, 14739-14760, https://doi.org/10.1029/JD092iD12p14739, 1987.

Kaseke, K. F., Mills, A. J., Brown, R., Esler, K. J., Henschel, J. R., and Seely, M. K.: A Method for Direct Assessment of the "Non Rainfall" Atmospheric Water Cycle: Input and Evaporation From the Soil, Pure and Applied Geophysics, 169, 847-857, https://doi.org/10.1007/s00024-011-0328-9, 2012.

Kaseke, K. F., Wang, L. X., and Seely, M. K.: Nonrainfall water origins and formation mechanisms, Science Advances, 3, https://doi.org/10.1126/sciadv.1603131, 2017.

Keeling, C. D.: The Concentration and Isotopic Abundances of Atmospheric Carbon Dioxide in Rural Areas, Geochimica Et Cosmochimica Acta, 13, 322-334, https://doi.org/10.1016/0016-7037(58)90033-4, 1958.

https://doi.org/10.5194/hess-2020-493
Preprint. Discussion started: 13 October 2020

Kelliher, F. M., Leuning, R., and Schulze, E. D.: Evaporation and Canopy Characteristics of Coniferous Forests and Grasslands, Oecologia, 95, 153-163, https://doi.org/10.1007/BF00323485, 1993.

Kidron, G. J., Herrnstadt, I., and Barzilay, E.: The role of dew as a moisture source for sand microbiotic crusts in the Negev Desert, Israel, Journal of Arid Environments, 52, 517-533, https://doi.org/10.1006/jare.2002.1014, 2002.

Lai, C. T. and Ehleringer, J. R.: Deuterium excess reveals diurnal sources of water vapor in forest air, Oecologia, 165, 213-223, https://doi.org/10.1007/s00442-010-1721-2, 2011.

Lai, C. T., Ehleringer, J. R., Bond, B. J., and U, K. T. P.: Contributions of evaporation, isotopic non-steady state transpiration and atmospheric mixing on the $\delta^{18}O$ of water vapour in Pacific Northwest coniferous forests, Plant Cell and Environment, 29, 77-94, https://doi.org/10.1111/j.1365-3040.2005.01402.x, 2006.

Lee, H., Smith, R., and Williams, J.: Water vapour $^{18}O/^{16}O$ isotope ratio in surface air in New England, USA, Tellus Series B-Chemical and Physical Meteorology, 58, 293-304, https://doi.org/10.1111/j.1600-0889.2006.00191.x, 2006.

Lee, X., Griffis, T. J., Baker, J. M., Billmark, K. A., Kim, K., and Welp, L. R.: Canopy-scale kinetic fractionation of atmospheric carbon dioxide and water vapor isotopes, Global Biogeochemical Cycles, 23, n/a-n/a, https://doi.org/10.1029/2008GB003331, 2009.

López, A., Molina-Aiz, F. D., Valera, D. L., and Peña, A.: Determining the emissivity of the leaves of nine horticultural crops by means of infrared thermography, Scientia Horticulturae, 137, 49-58, https://doi.org/10.1016/j.scienta.2012.01.022, 2012.

Malek, E., McCurdy, G., and Giles, B.: Dew contribution to the annual water balances in semi-arid desert valleys, Journal of Arid Environments, 42, 71-80, https://doi.org/10.1006/jare.1999.0506, 1999.

McHugh, T. A., Morrissey, E. M., Reed, S. C., Hungate, B. A., and Schwartz, E.: Water from air: an overlooked source of moisture in arid and semiarid regions, Scientific Reports, 5, 13767, https://doi.org/10.1038/srep13767, 2015.

Meng, Y. and Wen, X. F.: Characteristics of dew events in an arid artificial oasis cropland and a sub-humid cropland in China, Journal of Arid Land, 8, 399-408, https://doi.org/10.1007/s40333-016-0006-y, 2016.

Merlivat, L.: Molecular diffusivities of $H_2{}^{16}O$, $HD^{16}O$, and $H_2{}^{18}O$ in gases, The Journal of Chemical Physics, 69, 2864-2871, https://doi.org/10.1063/1.436884, 1978.

Monteith, J. L.: Dew, Quarterly Journal of the Royal Meteorological Society, 83, 322-341, https://doi.org/10.1002/qj.49708335706, 1957.

Monteith, J. L. and Unsworth, M. H.: Chapter 16 - Micrometeorology: (i) Turbulent Transfer, Profiles, and Fluxes, in: Principles of Environmental Physics (Fourth Edition), edited by: Monteith, J. L. and Unsworth, M. H., Academic Press, Boston, 289-320, https://doi.org/10.1016/B978-0-12-386910-4.00016-0, 2013.

Moore, C. J.: A comparative study of radiation balance above forest and grassland, Quarterly Journal of the Royal Meteorological Society, 102, 889-899, https://doi.org/10.1002/qj.49710243416, 1976.

Oke, T. R.: Boundary layer climates, 2nd Edition ed., Routledge, London, https://doi.org/10.4324/9780203407219, 2002.

Oke, T. R.: Temperature Profile near Ground on Calm Clear Nights, Quarterly Journal of the Royal Meteorological Society, 96, 14-&, https://doi.org/10.1002/qj.49709640703, 1970.

Parkes, S. D., McCabe, M. F., Griffiths, A. D., Wang, L., Chambers, S., Ershadi, A., Williams, A. G., Strauss, J., and Element, A.: Response of water vapour D-excess to land–atmosphere interactions in a semi-arid environment, Hydrology and Earth System Sciences, 21, 533-548, http://dx.doi.org/10.5194/hess-2016-271, 2017.

Philip, J. R. and De Vries, D. A.: Moisture movement in porous materials under temperature gradients, Eos, Transactions American Geophysical Union, 38, 222-232, https://doi.org/10.1029/TR038i002p00222, 1957.

Phillips, D. L., Newsome, S. D., and Gregg, J. W.: Combining sources in stable isotope mixing models: alternative methods, Oecologia, 144, 520-527, https://doi.org/10.1007/s00442-004-1816-8, 2005.

Prechsl, U. E., Burri, S., Gilgen, A. K., Kahmen, A., and Buchmann, N.: No shift to a deeper water uptake depth in response to summer drought of two lowland and sub-alpine C_3-grasslands in Switzerland, Oecologia, 177, 97-111, https://doi.org/10.1007/s00442-014-3092-6, 2015.

Prechsl, U. E., Gilgen, A. K., Kahmen, A., and Buchmann, N.: Reliability and quality of water isotope data collected with a lowbudget rain collector, Rapid Communications in Mass Spectrometry, 28, 879-885, https://doi.org/10.1002/rcm.6852, 2014.

Priestley, C. H. B. and Taylor, R. J.: On the Assessment of Surface Heat Flux and Evaporation Using Large-Scale Parameters, Mon Weather Rev, 100, 81-92, https://doi.org/10.1175/1520-0493(1972)100<0081:OTAOSH>2.3.CO;2, 1972.

R Core Team. R: A language and environment for statistical computing, https://www.R-project.org/, 2020.

Riedl, A., Li, Y., Buchmann, N., and Eugster, W.: High accuracy weighing micro-lysimeter system for long-term measurements of non-rain water inputs to short-statured grasslands. In: Journal of Hydrology, (submitted), 2020.

Roth, K.: Bodenkartierung und GIS-basierte Kohlenstoffinventur von Graslandböden: Untersuchungen an den ETH-Forschungsstationen Chamau und Früebüel (ZG, Schweiz), 2006. University of Zurich, Switzerland, 2006.

Schreel, J. D. M. and Steppe, K.: Foliar Water Uptake in Trees: Negligible or Necessary?, Trends in Plant Science, 25, 590-603, https://doi.org/10.1016/j.tplants.2020.01.003, 2020.

Spiegel, J. K., Aemisegger, F., Scholl, M., Wienhold, F. G., Collett, J. L., Lee, T., van Pinxteren, D., Mertes, S., Tilgner, A., Herrmann, H., Werner, R. A., Buchmann, N., and Eugster, W.: Temporal evolution of stable water isotopologues in cloud droplets in a hill cap cloud in central Europe (HCCT-2010), Atmospheric Chemistry and Physics, 12, 11679-11694, https://doi.org/10.5194/acp-12-11679-2012, 2012.

Stull, R. B.: Stable Boundary Layer, in: An Introduction to Boundary Layer Meteorology, edited by: Stull, R. B., Springer, Dordrecht, Dordrecht, 499-543, https://doi.org/10.1007/978-94-009-3027-8_12, 1988.

Thurnherr, I., Kozachek, A., Graf, P., Weng, Y., Bolshiyanov, D., Landwehr, S., Pfahl, S., Schmale, J., Sodemann, H., Steen-Larsen, H. C., Toffoli, A., Wernli, H., and Aemisegger, F.: Meridional and vertical variations of the water vapour isotopic composition in the marine boundary layer over the Atlantic and Southern Ocean, Atmos. Chem. Phys., 20, 5811-5835, https://doi.org/10.5194/acp-20-5811-2020, 2020.

Tomaszkiewicz, M., Abou Najm, M., Zurayk, R., and El-Fadel, M.: Dew as an adaptation measure to meet water demand in agriculture and reforestation, Agricultural and Forest Meteorology, 232, 411-421, https://doi.org/10.1016/j.agrformet.2016.09.009, 2017.

Tombrou, M., Founda, D., and Boucouvala, D.: Nocturnal boundary layer height prediction from surface routine meteorological data, Meteorology and Atmospheric Physics, 68, 177-186, https://doi.org/10.1007/BF01030209, 1998.

Ucles, O., Villagarcia, L., Canton, Y., and Domingo, F.: Microlysimeter station for long term non-rainfall water input and evaporation studies, Agricultural and Forest Meteorology, 182, 13-20, https://doi.org/10.1016/j.agrformet.2013.07.017, 2013.

Wang, C., Cen, Y., Liu, M., and Bowler, P.: Formation and influencing factors of dew in sparse elm woods and grassland in a semi-arid area, Acta Ecologica Sinica, 37, 125-132, https://doi.org/10.1016/j.chnaes.2017.06.004, 2017.

Welp, L. R., Lee, X., Griffis, T. J., Wen, X.-F., Xiao, W., Li, S., Sun, X., Hu, Z., Val Martin, M., and Huang, J.: A meta-analysis of water vapor deuterium-excess in the midlatitude atmospheric surface layer, Global Biogeochemical Cycles, 26, https://doi.org/10.1029/2011GB004246, 2012.

Wen, X. F., Lee, X., Sun, X. M., Wang, J. L., Hu, Z. M., Li, S. G., and Yu, G. R.: Dew water isotopic ratios and their relationships to ecosystem water pools and fluxes in a cropland and a grassland in China, Oecologia, 168, 549-561, https://doi.org/10.1007/s00442-011-2091-0, 2012.

Werner, R. A. and Brand, W. A.: Referencing strategies and techniques in stable isotope ratio analysis, Rapid Communications in Mass Spectrometry, 15, 501-519, https://doi.org/10.1002/rcm.258, 2001.

Williams, C. A., Reichstein, M., Buchmann, N., Baldocchi, D., Beer, C., Schwalm, C., Wohlfahrt, G., Hasler, N., Bernhofer, C., Foken, T., Papale, D., Schymanski, S., and Schaefer, K.: Climate and vegetation controls on the surface water balance:

https://doi.org/10.5194/hess-2020-493
Preprint. Discussion started: 13 October 2020

Synthesis of evapotranspiration measured across a global network of flux towers, Water Resources Research, 48, https://doi.org/10.1029/2011WR011586, 2012.

Wolf, S., Eugster, W., Ammann, C., Häni, M., Zielis, S., Hiller, R., Stieger, J., Imer, D., Merbold, L., and Buchmann, N.: Contrasting response of grassland versus forest carbon and water fluxes to spring drought in Switzerland, Environmental Research Letters, 8, 035007, https://doi.org/10.1088/1748-9326/8/3/035007, 2013.

Yakir, D. and Sternberg, L. d. S. L.: The use of stable isotopes to study ecosystem gas exchange, Oecologia, 123, 297-311, https://doi.org/10.1007/s004420051016, 2000.

Yepez, E. A., Williams, D. G., Scott, R. L., and Lin, G.: Partitioning overstory and understory evapotranspiration in a semiarid savanna woodland from the isotopic composition of water vapor, Agricultural and Forest Meteorology, 119, 53-68, https://doi.org/10.1016/S0168-1923(03)00116-3, 2003.

Zeeman, M. J., Hiller, R., Gilgen, A. K., Michna, P., Plüss, P., Buchmann, N., and Eugster, W.: Management and climate impacts on net CO_2 fluxes and carbon budgets of three grasslands along an elevational gradient in Switzerland, Agricultural and Forest Meteorology, 150, 519-530, https://doi.org/10.1016/j.agrformet.2010.01.011, 2010.

https://doi.org/10.5194/hess-2020-493
Preprint. Discussion started: 13 October 2020

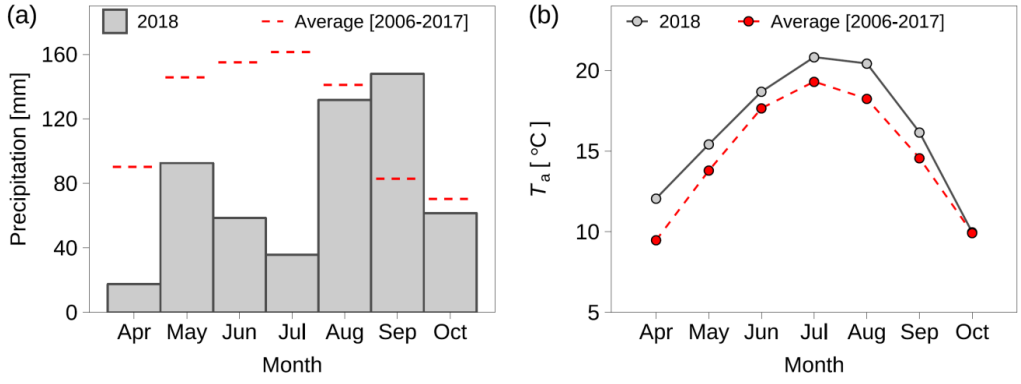

Figure 1. (**a**) Monthly precipitation and (**b**) monthly average temperature (T_a) from April to October in 2018 as compared to the corresponding months over 2006–2017.

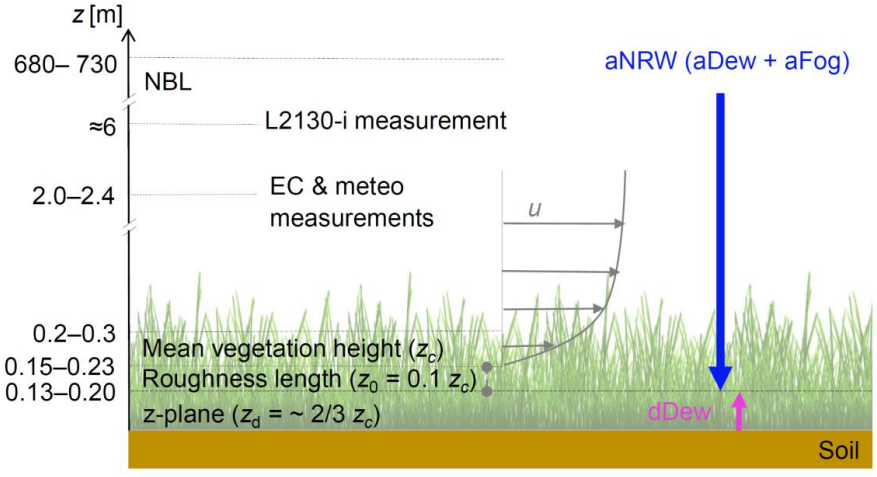

Figure 2. Simplified schematics of non-rainfall water (NRW) inputs adapted from Monteith and Unsworth (2013), and Oke (2002): "aDew" means dew formed from ambient water vapor, "aFog" means fog formed from ambient water vapor; "aDew" and "aFog" are both condensed from ambient water vapor, thus "aNRW" represents the condensation of ambient water vapor if either dew or fog input, or the combination of both was meant. ; "dDew" means dew formed from soil-diffusing vapor. The horizontal wind speed (u) is zero at $z_d + z_0$.

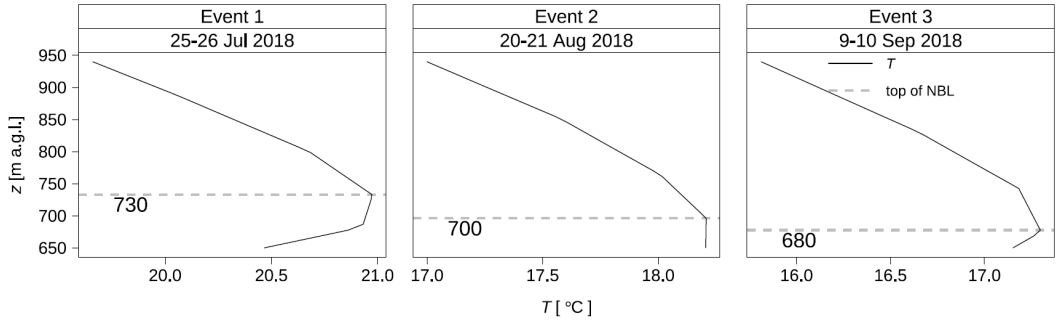

Figure 3. Nocturnal vertical profiles of air temperature (T) vs. height (z, in m a.g.l.) at 01:00 CET for the three events interpolated to the location of the measurement site based on ERA-5 reanalysis data (Hersbach et al., 2020; Horanyi, 2017).

https://doi.org/10.5194/hess-2020-493
Preprint. Discussion started: 13 October 2020

Hydrology and Earth System Sciences
Discussions
Open Access
EGU

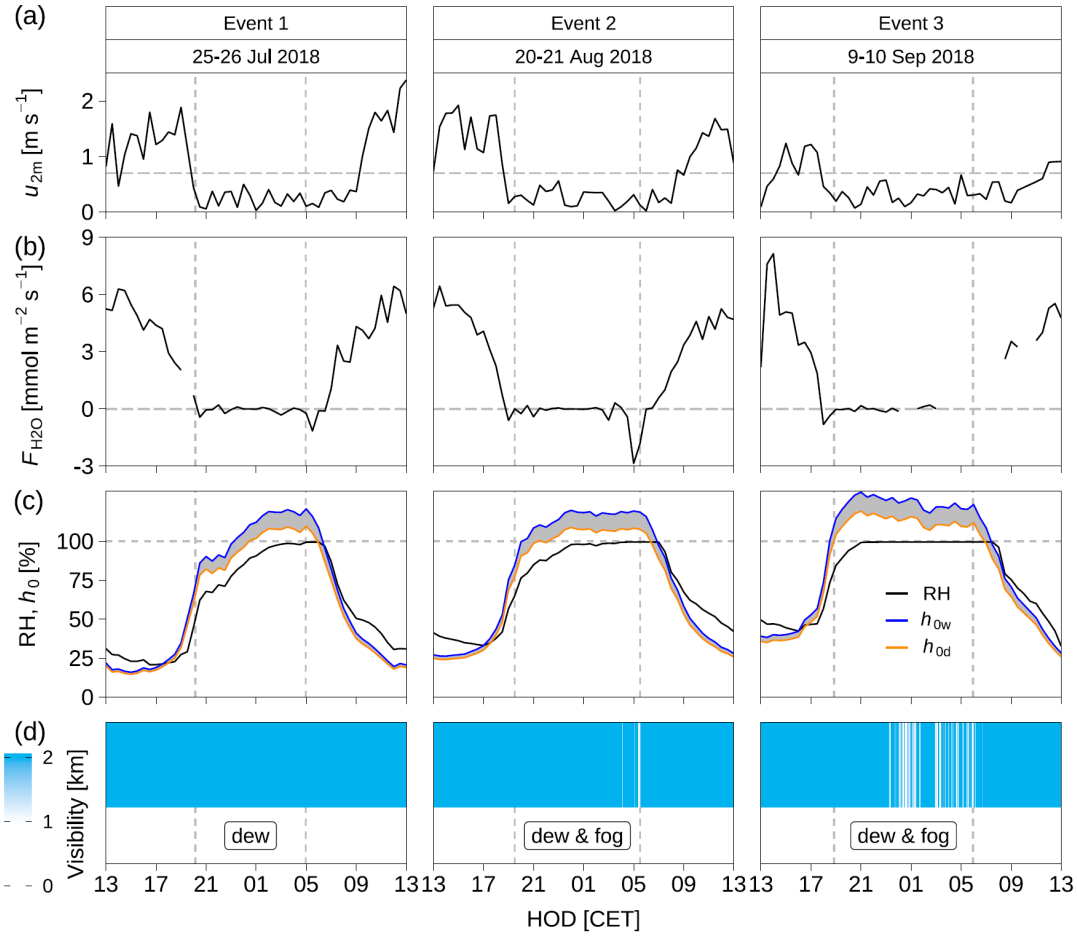

Figure 4. The meteorological and eddy-covariance (EC) measurements at the CH-CHA site. The 30 min averages of (**a**) horizontal mean wind speed at 2 m a.g.l. (u_{2m}), (**b**) H_2O flux at 2.4 m a.g.l. [F_{H2O}], (**c**) relative humidity at 2 m a.g.l. [RH], relative humidity with respect to the surface temperature [h_{0w} for wet surface, and h_{0d} for dry surface]; (**d**) 1 min averages of visibility (< 1 km with fog, and > 1 km with the absence of fog).

https://doi.org/10.5194/hess-2020-493
Preprint. Discussion started: 13 October 2020

Hydrology and Earth System Sciences
Discussions
Open Access
EGU

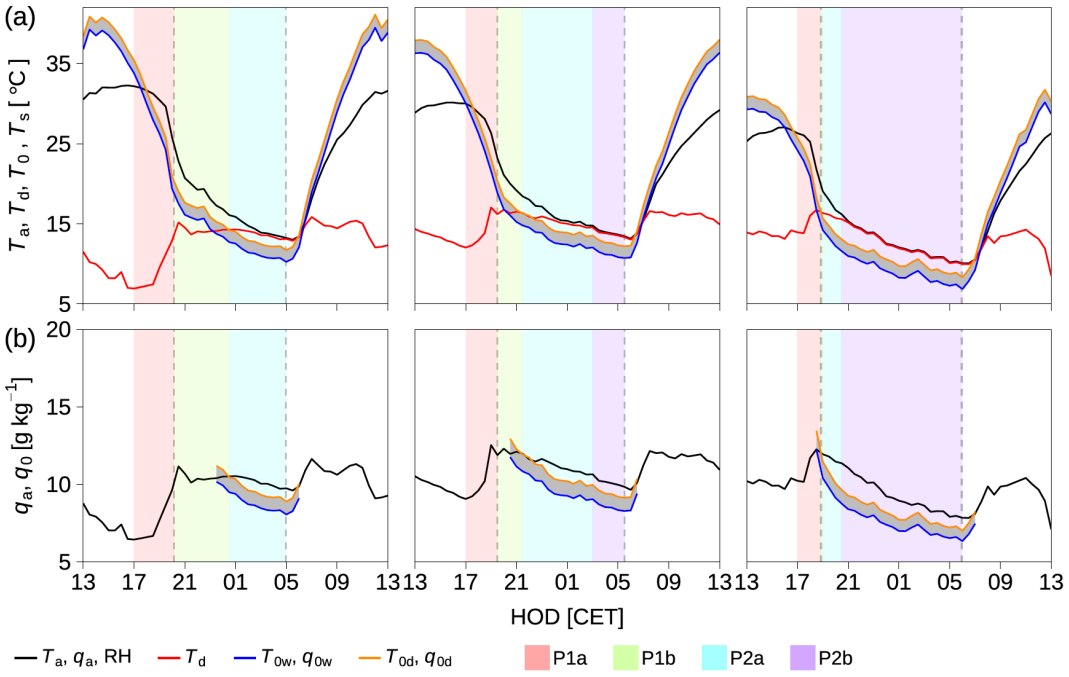

Figure 5. The meteorological and eddy covariance (EC) measurements at the CH-CHA site. The 30 min averages of (**a**) air temperature at 2 m a.g.l. [T_a], dew-point temperature of the ambient air [T_d], surface temperature for wet [T_{0w}], and dry [T_{0d}] assumptions, and (**b**) atmospheric specific humidity at 2.4 m a.g.l. [q_a], the saturation specific humidity respect to the surface temperature under wet [q_{0w}] and dry [q_{0d}] assumptions. P1a was from 17:00 CET until sunset with the weakened turbulence and increased specific humidity; P1b was a short-term variability of specific humidity; P2a was dew formation in unsaturated ambient air; P2b was dew and radiation fog in combination in saturated ambient air.

https://doi.org/10.5194/hess-2020-493
Preprint. Discussion started: 13 October 2020

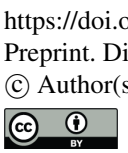

Hydrology and Earth System Sciences
Discussions
Open Access
EGU

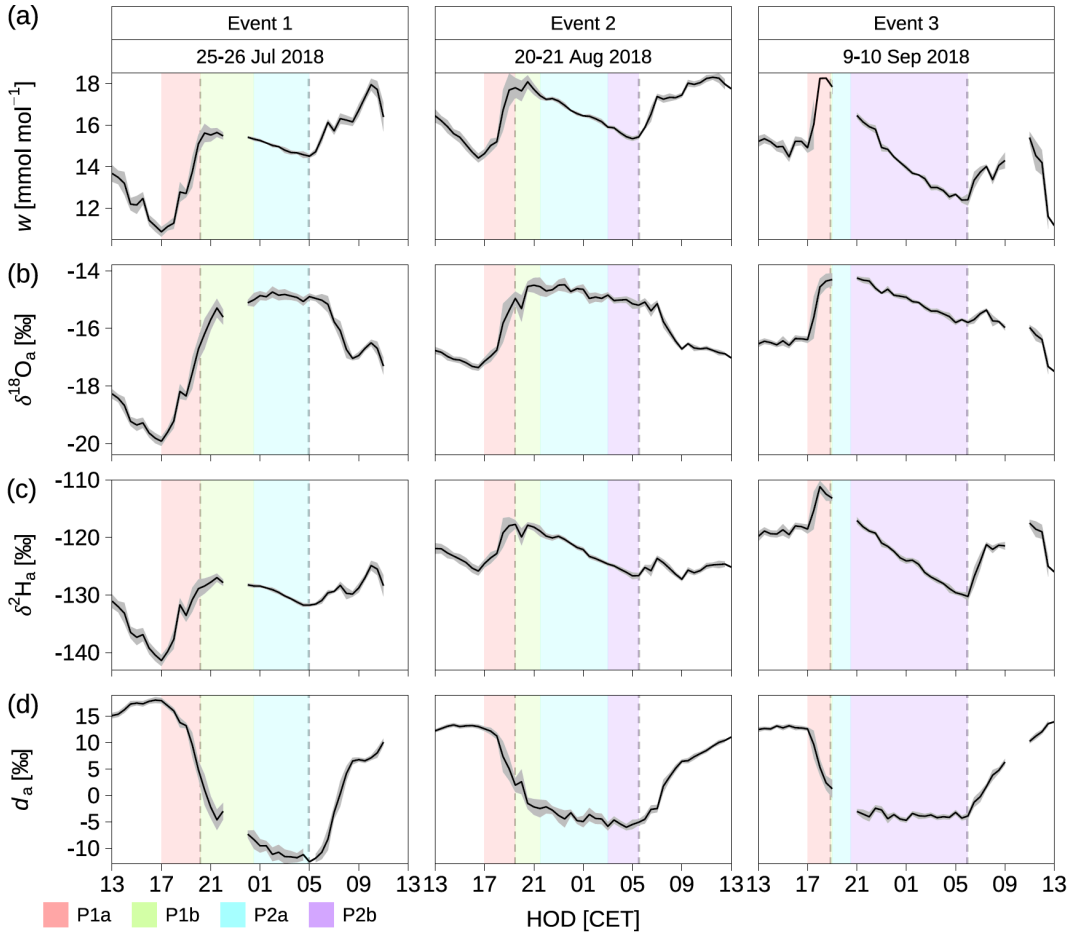

Figure 6. The volumetric mixing ratio and isotopic compositions for ambient water vapor. The 30 min averages and standard deviations of (**a**) volumetric ambient water vapor mixing ratio (w), and (**b-d**) the isotopic compositions of ambient water vapor ($\delta^{18}O_a$, $\delta^{2}H_a$, and d_a). P1a was from 17:00 CET until sunset with the weakened turbulence and increased specific humidity; P1b was a short-term variability of specific humidity; P2a was dew formation in unsaturated ambient air; P2b was dew and radiation fog in combination in saturated ambient air.

https://doi.org/10.5194/hess-2020-493
Preprint. Discussion started: 13 October 2020

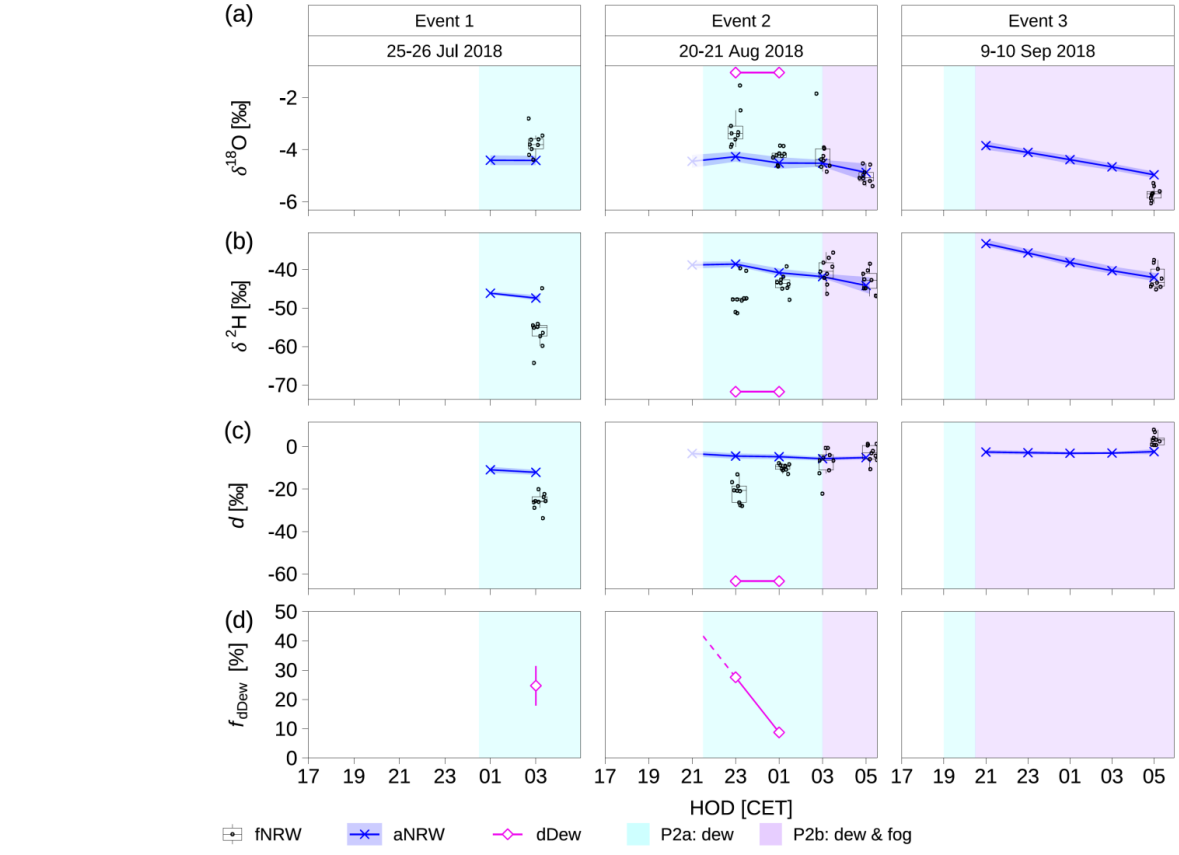

Figure 7. (**a–c**) Isotopic compositions of different non-rainfall water (fNRW, aNRW, and dDew), and (**d**) the proportions of dDew (f_{dDew}). "fNRW", the NRW on foliage; "aNRW", the NRW condensed from ambient water vapor; "dDew", the dew component condensed from soil-diffusing vapor. P2a was dew formation in unsaturated ambient air; P2b was dew and radiation fog in combination in saturated ambient air.

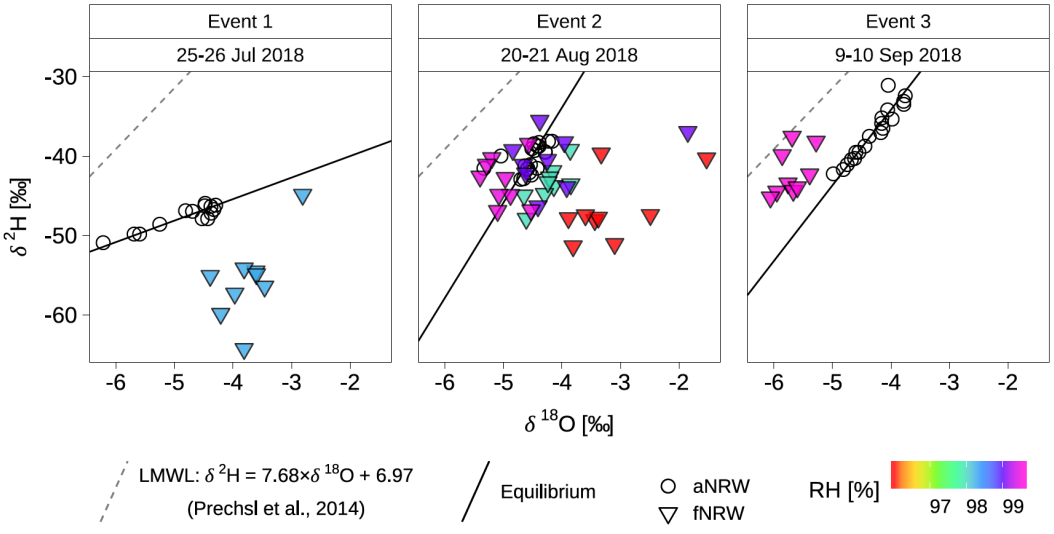

Figure 8. The relationship of δ^2H_{fNRW}–$\delta^{18}O_{fNRW}$ with respect to the orthogonal regression of δ^2H_{aNRW}–$\delta^{18}O_{aNRW}$ and local meteorological water line (LMWL: $\delta^2H = 7.68 \times \delta^{18}O + 6.97$, Prechsl et al. (2014)). "fNRW" means non-rainfall water (NRW) on foliage, and "aNRW" means the NRW equilibrium from ambient water vapor. "RH" is relative humidity at 2 m a.g.l..

https://doi.org/10.5194/hess-2020-493
Preprint. Discussion started: 13 October 2020

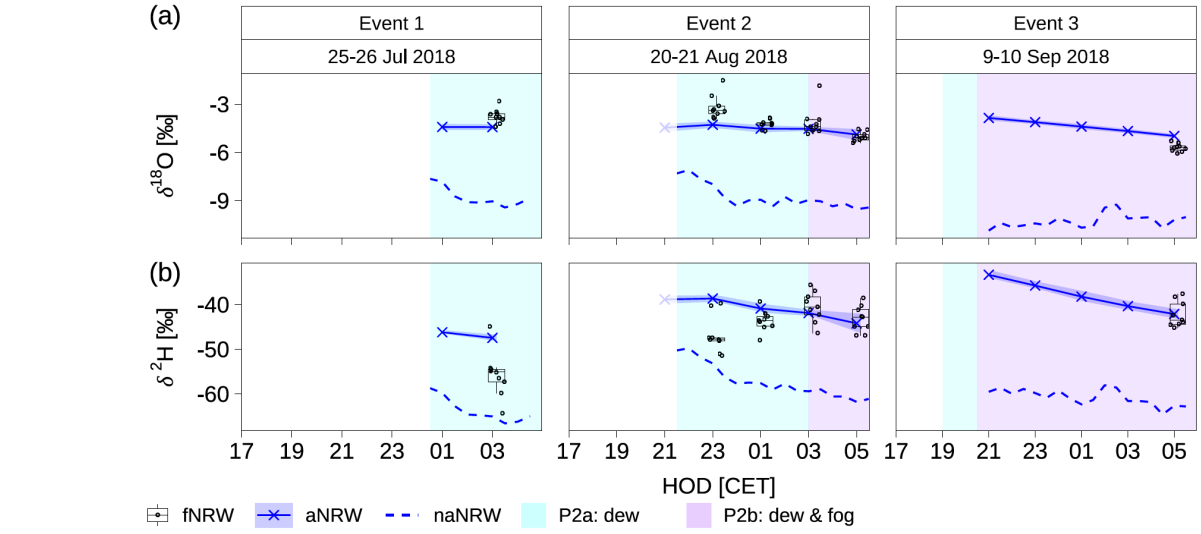

Figure 9. Comparing the isotopic compositions of the simulated NRW to the isotopic compositions of the NRW on foliage (δ_{fNRW}). The δ_{aNRW} was calculated from ambient water vapor δ_a considering equilibrium fractionation, and δ_{naNRW} was calculated from ambient water vapor δ_a considering both equilibrium and non-equilibrium fractionation). P2a was dew formation in unsaturated ambient air; P2b was dew and radiation fog in combination in saturated ambient air.

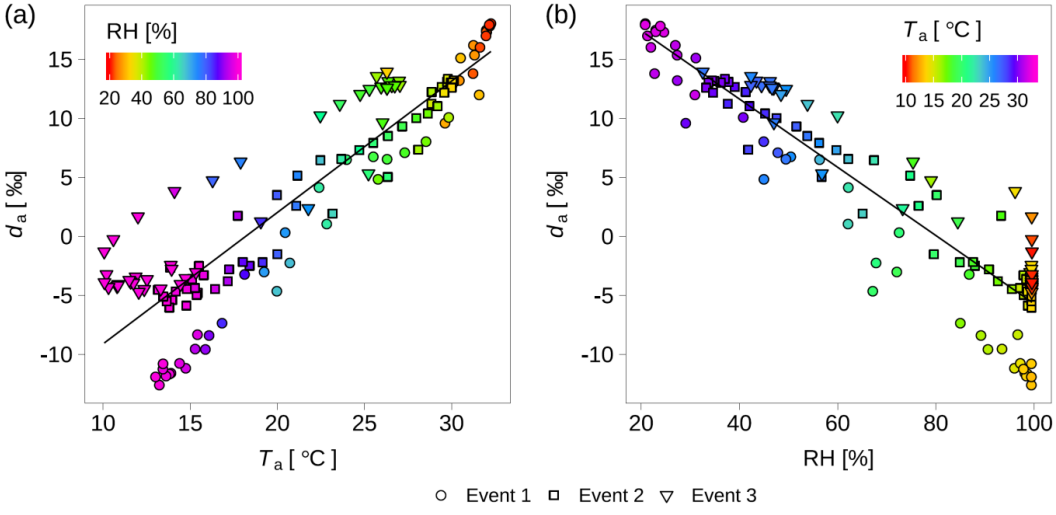

Figure 10. The relationships of (**a**) d_a– T_a and (**b**) d_a–RH for the 24 h measurements during the three events. The d_a is the deuterium excess of ambient water vapor; T_a is the ambient temperature at 2 m a.g.l.; RH is relative humidity at 2 m a.g.l..

https://doi.org/10.5194/hess-2020-493
Preprint. Discussion started: 13 October 2020

Hydrology and Earth System Sciences
Discussions
Open Access
EGU

Table 1. Partitioning the contribution s of dDew from a mix of dDew and aDew. The fNRW means the non-rainfall water (NRW) on foliage; aNRW represents either dew or radiation fog, or dew and radiation fog in combination condensed from ambient water vapor; dDew means dew condensed from soil-diffusing vapor; f_{dDew} means the proportion of dDew in total foliage NRW.

Event	Time	Isotope	fNRW	aNRW	dDew	f_{dDew}(%)
Event 1	3:00 CET	$\delta^{18}O$ (‰)	–3.8	–4.4±0.2	–1.0	18–31
		$\delta^{2}H$ (‰)	–55.1	–47.4±1.7	–71.8	
		d (‰)	–25.6	–12.1±1.3	–63.4	
Event 2	21:30 CET	No sampling, but extrapolating from 23:00 and 1:00 CET				42
	23:00 CET	$\delta^{18}O$ (‰)	–3.4	–4.3±0.2	–1.0	28
		$\delta^{2}H$ (‰)	–47.7	–38.6±0.7	–71.8	
		d (‰)	–20.7	–4.4±1.3	–63.4	
	1:00 CET	$\delta^{18}O$ (‰)	–4.2	–4.5±0.2	–1.0	9
		$\delta^{2}H$ (‰)	–43.5	–40.8±1.0	–71.8	
		d (‰)	–9.4	–4.7±1.1	–63.4	

Table 2. Estimating the potential non-rainfall water (NRW) gain of the three events in our study according to the condensation rate of Monteith (1957). The fNRW means the non-rainfall water (NRW) on foliage; aNRW represents either dew or radiation fog, or dew and radiation fog in combination condensed from ambient water vapor; dDew means dew condensed from soil-diffusing vapor.

Event	Period (h night^{-1})		Condensation rate following Monteith (1957) (mm h^{-1})		Potential NRW gain		
	dDew	aNRW	dDew	aNRW	dDew	aNRW	total
Event 1	4.0	4.0	0.01 – 0.02	0.004 – 0.035	0.04 – 0.08	0.02 – 0.14	0.06 – 0.22
Event 2	5.5	8.0	0.01 – 0.02	0.004 – 0.035	0.06 – 0.11	0.03 – 0.28	0.09 – 0.39
Event 3	0	10.5	0.01 – 0.02	0.004 – 0.035	0	0.04 – 0.37	0.04 – 0.37

Table 3. Evapotranspiration rate during the corresponding continuous no-rain periods of the three events processed from EC measurements.

Event	Corresponding continuous no-rain periods (yyyy-mm-dd)	Average daily (daytime) evapotranspiration (mm day^{-1})
Event 1	2018-07-23	2.7
	2018-07-24	3.3
	2018-07-25	3.3
	2018-07-26	3.4
	2018-07-27	3.0
Event 2	2018-08-18	2.6
	2018-08-19	2.8
	2018-08-20	3.0
	2018-08-21	2.9
Event 3	2018-09-08	3.1
	2018-09-09	2.7
	2018-09-10	2.1
	2018-09-11	2.0
	2018-09-12	1.7

https://doi.org/10.5194/hess-2020-493
Preprint. Discussion started: 13 October 2020

Hydrology and Earth System Sciences
Discussions
Open Access
EGU

Appendix

Appendix A: Measurements and samplings at the CH-CHA site

Figure A1. Measurements and sampling at the CH-CHA site (Satellite Image: © CNES /Spot Image/swisstopo, NPOC). "L2130-i" represents the isotopic compositions and mixing ratio measurements for ambient water vapor; "EC & meteo" represents the eddy-covariance and meteorological measurements; "Sampling of fNRW" represents the sampling of non-rainfall water droplets on foliage.

Appendix B: Meteorological and eddy covariance calculations

The saturation specific humidity [q_0, g kg^{-1}] for wet (q_{0w}) and dry (q_{0d}) vegetation surfaces was calculated after Campbell and Norman (1998) as:

$$q_0 = \frac{622 \cdot e_{s0}}{p - 0.378 \cdot e_{s0}} \quad , \tag{B1}$$

where p in hPa is air pressure, and e_{s0} in hPa is saturation vapor pressure at T_0 calculated after Tetens formula (Buck, 1981) as:

$$e_{s0} = 6.11 \cdot \exp\left(\frac{17.502 \cdot T_0}{T_0 + 240.97}\right) . \tag{B2}$$

The dew point temperature (T_d, °C) was calculated after Campbell and Norman (1998) as:

$$T_d = 240.97 \cdot \frac{\ln\left(\frac{e_{sa} \cdot RH}{6.11}\right)}{17.502 - \ln\left(\frac{e_{sa} \cdot RH}{6.11}\right)} \quad , \tag{B3}$$

where e_{sa} in hPa is saturation vapor pressure at T_a calculated after Tetens formula (Buck, 1981) as:

$$e_{sa} = 6.11 \cdot \exp\left(\frac{17.502 \cdot T_a}{T_a + 240.97}\right) . \tag{B4}$$

https://doi.org/10.5194/hess-2020-493
Preprint. Discussion started: 13 October 2020

Hydrology and Earth System Sciences
Discussions

Appendix C: Calculating the isotopic compositions of the NRW from the isotopic compositions of ambient water vapor under equilibrium fractionation

After Horita and Wesolowski (1994), the isotopic compositions of the NRW ($\delta^{18}O_{aNRW}$ and $\delta^{2}H_{aNRW}$) equilibrium from the isotopic compositions of ambient water vapor ($\delta^{18}O_a$ and $\delta^{2}H_a$) at surface temperature T_{0w} were calculated as:

$$\delta^{18}O_{aNRW}=\left(10^3+\delta^{18}O_a\right)\cdot\exp\left(0.35041\cdot\frac{10^6}{(T_{0w}+273.15)^3}-1.6664\cdot\frac{10^3}{(T_{0w}+273.15)^2}+\frac{6.7123}{T_{0w}+273.15}-\frac{7.685}{10^3}\right)-10^3\ , \quad (C1)$$

and

$$\delta^{2}H_{aNRW}=\left(10^3+\delta H_a\right)\cdot\exp\left(1.1588\frac{(T_{0w}+273.15)^3}{10^9}-1.6201\frac{(T_{0w}+273.15)^2}{10^6}+0.79484\cdot\frac{(T_{0w}+273.15)}{10^3}-0.16104+2.9992\cdot\frac{10^6}{(T_{0w}+273.15)^3}\right)-10^3\ . \quad (C2)$$

Appendix D: Simulating the isotopic compositions of the condensate from the isotopic compositions of ambient water vapor considering both equilibrium and non-equilibrium fractionation factors

In our results shown in Fig. 7, we assumed equilibrium fractionation was dominant during the condensation of ambient water vapor, hence we calculated $\delta^{18}O_{aNRW}$ and $\delta^{2}H_{aNRW}$ equilibrium from ambient water vapor (Figs. 7 and 9) using (Eqs. C1 – C2). Whereas, Wen et al. (2012) adopted the method to simulate the isotopic compositions of the NRW from ambient water vapor considering both equilibrium and non-equilibrium fractionation factors ($\delta^{18}O_{naNRW}$ and $\delta^{2}H_{naNRW}$ in Fig. 9). To compare these two methods, we applied the method by Wen et al. (2012) on our data, and the equations for calculating $\delta^{18}O_{naNRW}$ and $\delta^{2}H_{naNRW}$ was:

$$\delta_{naNRW}=\frac{\delta_a+\epsilon_{eq}/h_0+(1-h_0)\epsilon_k/h_0}{1+\epsilon_k/1000-(\epsilon_{eq}+\epsilon_k)\,(1/h_0)/1000} \quad (D1)$$

where ϵ_k is the non-equilibrium fractionation factor in permil, calculated from $\epsilon_k = m(1 - D_i/D_l) \times 1000$ ‰ following Lee et al. (2009), given D_i/D_l (^{18}O) = 0.9723, D_i/D_l (^{2}H) = 0.9755 following Merlivat (1978), and m = 0.67 for laminar flow following Dongmann et al. (1974); ϵ_{eq} is equilibrium fractionation factor in permil calculated from $(1 - 1/\alpha) \times 1000$ ‰ with α calculated as:

$$\alpha\,(^{18}O)=\exp\left(0.35041\cdot\frac{10^6}{(T_{0w}+273.15)^3}-1.6664\cdot\frac{10^3}{(T_{0w}+273.15)^2}+\frac{6.7123}{T_{0w}+273.15}-\frac{7.685}{10^3}\right) \quad (D2)$$

$$\alpha\,(^{2}H)=\exp\left(0.35041\cdot\frac{10^6}{(T_{0w}+273.15)^3}-1.6664\cdot\frac{10^3}{(T_{0w}+273.15)^2}+\frac{6.7123}{T_{0w}+273.15}-\frac{7.685}{10^3}\right) \quad (D3)$$

Appendix E. Soil vapor diffusion occurred as long as the temperature gradient generated

The dDew was condensed from soil-diffusing vapor, which occurred as long as the temperate gradient generated. The temperature gradient was largest at the land – atmosphere interface (Fig. 5a), but within the soil profile, temperate gradient also generated. The soil temperature at 5 cm, 10 cm, 15 cm, 20 cm, 30 cm, 40 cm, and 50 cm in depth were shown in Fig. E1 (ML2x, Delta-T Devices Ltd., Cambridge, United Kingdom).

https://doi.org/10.5194/hess-2020-493
Preprint. Discussion started: 13 October 2020

Hydrology and Earth System Sciences
Discussions
Open Access
EGU

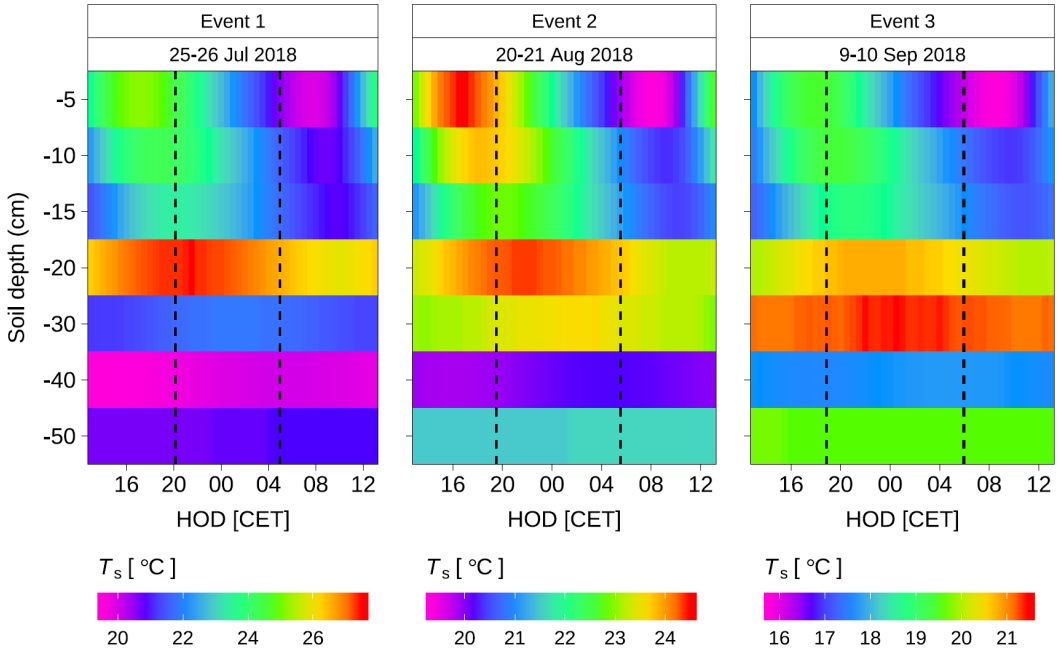

Figure E1. Soil temperature at different depths.